Assimilation of SMAP Brightness Temperature Observations in the GEOS Land-Atmosphere Data Assimilation System

Rolf H. Reichle, Sara Q. Zhang, Qing Liu, Clara S. Draper, Jana Kolassa, and Ricardo Todling

Abstract—**Errors in soil moisture adversely impact the modeling of land-atmosphere water and energy fluxes and, consequently, near-surface atmospheric conditions in atmospheric data assimilation systems (ADAS). To mitigate such errors, a land surface analysis is included in many such systems, although not yet in the currently operational NASA Goddard Earth Observing System (GEOS) ADAS. This study investigates the assimilation of L-band brightness temperature (Tb) observations from the Soil Moisture Active Passive (SMAP) mission in the GEOS weakly-coupled land-atmosphere data assimilation system (LADAS) during boreal summer 2017. The SMAP Tb analysis improves the correlation of LADAS surface and root-zone soil moisture vs. in situ measurements by ~0.1-0.26 over that of ADAS estimates; the unbiased root-mean-square error (ubRMSE) of LADAS soil moisture is reduced by 0.002-0.008 m^3/m^3 from that of ADAS. Furthermore, the global land average RMSE vs. in situ measurements of screen-level air specific humidity (q2m) and daily maximum temperature (T2m$_{max}$) is reduced by 0.05 g/kg and 0.04 K, respectively, for LADAS compared to ADAS estimates. Regionally, the RMSE of LADAS q2m and T2m$_{max}$ is improved by up to 0.4 g/kg and 0.3 K, respectively. Improvement in LADAS specific humidity extends into the lower troposphere (below ~700 mb), with relative improvements in bias of 15-25%, although LADAS air temperature bias slightly increases relative to that of ADAS. Finally, the root-mean-square of the LADAS Tb observation-minus-forecast residuals is smaller by up to ~0.1 K than in a land-only assimilation system, corroborating the positive impact of the Tb analysis on the modeled land-atmosphere coupling.**

Index Terms—**Microwave remote sensing, soil moisture, data assimilation, soil moisture active passive (SMAP).**

I. Introduction

S OIL moisture plays an important role in the Earth's energy, water, and carbon cycles through its control on photosynthesis and evapotranspiration, which in turn impact atmospheric boundary layer dynamics. Consequently, the accurate modeling of soil moisture is critical for improving weather and seasonal climate predictions [1]-[5]. But soil moisture processes and land-atmosphere interactions are highly complex and heterogeneous, and current models are subject to large uncertainties [6]. Errors in modeled land surface fields can be reduced through the assimilation of land surface observations [7]. For example, near-surface air temperature and humidity are sensitive to soil moisture under certain atmospheric conditions. Since the 1990s, many weather centers have been using screen-level (2-m) temperature and humidity measurements to constrain the simulated soil moisture and thereby improve medium-range forecasts of near-surface temperature and precipitation in their operational data assimilation systems [8]-[16].

More recently, satellite observations suitable or specifically designed for the estimation of global surface soil moisture have become available. The sensors and platforms of most relevance for land assimilation include the Advanced Scatterometer (ASCAT; since 2007) [17], [18], the Soil Moisture and Ocean Salinity (SMOS) mission (since 2010) [19], [20], and the Soil Moisture Active Passive (SMAP) mission (since 2015) [21], [22]. ASCAT measures C-band (5.3 GHz) radar backscatter, which is sensitive to moisture in the top ~1 cm soil layer, whereas SMOS and SMAP collect L-band (1.4 GHz) passive microwave brightness temperature (Tb) observations, which are highly sensitive to moisture in the top ~5 cm soil layer. Soil moisture retrievals from these sensors are now assimilated in the operational data assimilation systems at several weather centers, with positive or neutral impact on short- and medium-range forecasts of screen-level temperature and humidity [12], [16], [23]-[26].

SMAP observations have been used operationally since 2015 in the NASA Goddard Earth Observing System (GEOS) land data assimilation system (LDAS) to generate the SMAP Level-4 Soil Moisture (L4_SM) product [27]. Using ensemble-based techniques, the L4_SM algorithm optimally combines the information from SMAP Tb observations, the land surface model, and its surface meteorological forcing data. The resulting L4_SM soil moisture estimates have the advantage of

complete coverage in space and time, including the propagation of surface layer information from SMAP observations into deeper soil layers, and were shown to improve upon model-only soil moisture estimates [28], [29].

The L4_SM algorithm is a stand-alone, land-only data assimilation system forced with surface meteorological data from the quasi-operational, near-real time GEOS Forward Processing (FP) atmospheric data assimilation system (ADAS) [30]. The L4_SM information does not, however, feed back into the FP ADAS, which does not yet include a land surface analysis. Likewise, the GEOS ADAS version that generates the Modern-Era Retrospective Analysis for Research and Applications, version 2 (MERRA-2) [31] product does not include a land surface analysis, although the MERRA-2 system uses gauge-based precipitation to force the land surface, which mitigates some of the errors in the modeled soil moisture [32].

To explore the potential benefit of assimilating land surface observations in future NASA reanalyses, [33] (hereinafter DR19) developed a weakly coupled GEOS land-atmosphere data assimilation system (LADAS). In this weakly coupled framework, the atmospheric analysis and the land surface analysis are performed separately, without sharing observation or model background error information. The two-way interactions of the LDAS and ADAS subsystems in the LADAS are predicated on the 6-hour ADAS assimilation cycle and consist of (i) forcing the LDAS with surface meteorological data from the ADAS and (ii) forcing the ADAS with soil moisture correction terms generated by the LDAS (section II). With the ADAS subsystem of their LADAS configured to match that of MERRA-2, DR19 showed that the assimilation of soil moisture retrievals from ASCAT and SMOS improved estimates of screen-level temperature and humidity in the LADAS when compared to the control ADAS experiment without a land surface analysis.

SMAP can provide more accurate and more spatially complete soil moisture information than ASCAT or SMOS [34]-[36]. The primary objective of the present paper is to determine by how much the assimilation of SMAP Tb observations in the GEOS LADAS can improve the simulated soil moisture and near-surface atmospheric variables. The design of the LADAS and the overall experimentation approach are as in DR19. However, the present study differs from DR19 in three key aspects. First, the LDAS used here employs a spatially distributed ("3-dimensional") land analysis and directly assimilates SMAP Tb observations (that is, radiances) after a seasonally varying Tb bias correction as in the L4_SM algorithm (section II-B), whereas DR19 used a local ("1-dimensional") assimilation of ASCAT and SMOS soil moisture retrievals after cumulative distribution function matching [37]. Both radiance and retrieval assimilation are commonly used, although the two approaches differ in how the observations add value to the system [38]. Second, compared to DR19 the LADAS used here includes improved atmospheric and land models [28], [39], and the atmospheric analysis in the ADAS now assimilates an expanded suite of atmospheric observations (section II-B). Third, unlike DR19, the present study does not use gauge-based precipitation to force the land surface because

the present study focuses on the near-real time GEOS FP weather analysis, for which the gauge-based precipitation data do not meet latency requirements. The latter two differences from DR19 have a competing impact on the ADAS baseline skill against which improvements from SMAP data assimilation are measured.

As will be demonstrated in this study, SMAP assimilation in the LADAS yields improved estimates of soil moisture and near-surface atmospheric variables compared to the ADAS baseline, and the skill improvements from SMAP assimilation are slightly better than those documented by DR19 for ASCAT and SMOS assimilation. An enhanced GEOS land-atmosphere analysis has the potential to improve a range of GEOS data products, including the near-real time GEOS FP weather analysis and prediction products, the GEOS subseasonal-to-seasonal forecasts, and future GEOS-based reanalysis products.

The paper is organized as follows. Section II describes the data and methods that are used in the data assimilation experiments and for the evaluation. Section III assesses the results of the assimilation experiments. Finally, section IV provides a summary and plans for future development.

II. Data and Methods

A. SMAP Observations

Since 31 March 2015, the SMAP observatory has been measuring L-band (1.4 GHz) passive microwave Tb with full global coverage every 2-3 days. The SMAP Tb observations are highly sensitive to surface soil moisture and temperature in regions with less than ~5 kg m^{-2} vegetation water content. The SMAP Tb observations used here are from the L1C_TB Version 4 product [40] on the 36-km Equal Area Scalable Earth version 2 (EASEv2) grid [41]. Prior to assimilation, we average the fore- and aft-looking Tb data. We assimilate horizontally (H) and vertically (V) polarized Tb observations from descending and ascending half-orbits (~6am/pm local equator overpass time, respectively).

The total Tb observation error standard deviation is prescribed to a constant value of 4 K, which includes the instrument error and the representativeness error associated with the forward radiative transfer model that converts the simulated soil moisture and temperature into model Tb estimates (section II-B). The observation errors of H- and V-polarization Tb are assumed to be uncorrelated. The Tb observations are screened in a quality control procedure before they are accepted into the assimilation. For instance, we exclude observations that are flagged for non-optimal quality in the L1C_TB product or fall outside the natural range (100-320 K). Moreover, we exclude observations for times and locations with frozen or snow-covered surface conditions (based on soil temperature and snow mass estimates in the LDAS) when the radiative transfer model is not valid [28]. On average during the June–August (JJA) 2017 experiment period, approximately one pair of H- and V-polarization observations from each 36-km land grid cell in the L1C_TB product was assimilated every day in the mid-latitudes, with higher counts in the high latitudes and lower counts in the Tropics owing to SMAP's orbital

characteristics.

B. Data Assimilation Systems

1) Atmospheric Data Assimilation

In this study, we used the GEOS ADAS version 5.26.4. As in MERRA-2 and DR19, the AGCM was set up on a 0.5-degree resolution ("c180") cubed-sphere horizontal grid with 72 hybrid-eta levels from the surface to 0.01 hPa, with a lowest atmospheric model layer centered at ~40-60 m above the surface. Model output was written on a 0.5-degree by 0.625-degree latitude-longitude grid. The latter grid was also used for the atmospheric data assimilation, which used a 3-dimensional variational deterministic (3D-Var) analysis. Each 6-hour assimilation cycle starts with an atmospheric analysis that merges observations with a model background from the previous cycle's AGCM "first guess" background forecast (or "Predictor" segment) and thereby produces atmospheric correction terms (or "increments"). Next, another AGCM simulation (or "Corrector" segment) for the same 6-hour period is forced with tendency terms derived from the atmospheric analysis increments. Finally, the next Predictor segment (i.e., an AGCM forecast for the next 6-hour period) is generated to complete the cycle. See Fig. 1 of [42] for a schematic.

Whereas the ADAS resolution and the 3D-Var atmospheric analysis method used here match that of MERRA-2 and DR19, the ADAS version 5.26.4 used in the present study includes several important upgrades from that of MERRA-2 and DR19 (version 5.12.4). Specifically, the AGCM used here includes important upgrades in the land physics [28], [43], the atmospheric physics and radiation [39], [44], [45], and the atmosphere-ocean interface parameterization [46]. Furthermore, the atmospheric analysis now benefits from an expanded set of assimilated atmospheric observations taken here from the GEOS operational data stream as in FP (most notably, now including data from the Special Sensor Microwave Imager Sounder), an ocean skin temperature analysis [46], re-tuned background error covariances, the use of inter-channel observation error correlations for handling data from the Atmospheric Infrared Sounder and the Infrared Atmospheric Sounding Interferometer [47], and the application of a digital filter to the atmospheric analysis tendencies in the incremental analysis update procedure [48], [49]. Finally, unlike MERRA-2 and DR19, the present study does not use gauge-based precipitation data to correct the land surface forcing in the ADAS (to be consistent with FP latency requirements).

2) Land Data Assimilation

The GEOS LDAS consists of a stochastic ensemble Kalman filter (EnKF) [38], [50], [51] and the Catchment land surface model [52], [53]. Unlike traditional, layer-based land surface models, the Catchment model explicitly accounts for spatial variations in soil moisture and water table depth within each "tile" (or computational unit) of a watershed based on its topographic statistics. Specifically, the Catchment model simulates soil moisture in three nested layers for the surface (0-5 cm), root-zone (0-100 cm), and profile (0 cm to bedrock),

based on the spatially varying equilibrium soil moisture profile (where gravity balances capillary forces) and deviations thereof in the surface and root-zone layers. The model prognostic variables accounting for these deviations are the "surface excess" and "root-zone excess", respectively. A third model prognostic variable, the "catchment deficit", tracks the amount of water that would be needed to bring the catchment to full saturation. Volumetric soil moisture estimates in the three nested layers are diagnosed from these three model prognostic variables. The model also includes a six-layer heat diffusion model for soil temperature and a three-layer snow model component that describes the state of the snowpack in terms of snow water equivalent, snow depth, and snow heat content [54].

The core of the observation operator is a zero-order "tau-omega" radiative transfer model [55] that converts the simulated soil moisture and temperature into model estimates of the observed L-band Tb. Key input parameters to the radiative transfer model, such as the microwave surface roughness, vegetation structure parameters, and scattering albedo were calibrated using multi-angular SMOS Tb observations [28], [56].

The LDAS used here matches that of the Version 4 L4_SM algorithm [28], except that here the Catchment model is set up in the 1/2-degree cube-sphere tile space, uses look-up table values for tree height to compute surface aerodynamic roughness lengths, and employs the Helfand surface turbulence scheme [28], [43]. These modifications are necessary to make the Catchment model version and configuration in the LDAS fully consistent with that in the AGCM of the ADAS. The Catchment model is driven with surface meteorological forcing data from the ADAS. Ensemble spread in the land states is achieved by applying random perturbations to select surface meteorological forcing data and land model prognostic variables as described in [27]. Every 3 hours, the available SMAP Tb observations and corresponding model forecasts are used in an EnKF analysis, which computes increments for the surface excess, root-zone excess, surface temperature, and surface soil heat content of each ensemble member. These increments are then immediately applied to correct the soil moisture and temperature state in the respective Catchment model ensemble members.

Seasonally-varying bias in the modeled Tb is addressed prior to data assimilation by converting the Tb observations and the model-simulated Tb into anomalies from their respective mean seasonal cycles. This is done separately for each grid cell, polarization, and orbit direction [38]. Here, the required mean seasonal cycles were estimated from SMAP observations available for the period from April 2015 to June 2020. The mean seasonal cycles for the model-simulated Tb were sampled at the times and locations of the SMAP overpasses from an "Open Loop" ensemble simulation of the land modeling system (that is, with the application of perturbations but without SMAP Tb assimilation; section II-C). This approach ensures a largely unbiased land surface analysis, at the expense of not correcting potential errors in the model's mean seasonal cycle.

3) Coupled Land and Atmospheric Data Assimilation

The GEOS LADAS used here is built on the recent GEOS ADAS and LDAS versions described above but otherwise follows the basic structure described in DR19; their Fig. 1 provides a schematic diagram. Building on the 6-hour Predictor/Corrector cycle of the ADAS described above, the ADAS and LDAS subsystems are weakly coupled through the land-atmosphere interactions encoded in the AGCM, which provides surface meteorological forcing data to and receives land analysis increments from the LDAS subsystem. Specifically, in parallel to the atmospheric analysis, surface meteorological forcing data from the previous cycle's AGCM background forecast (i.e., Predictor segment) are used to drive a Catchment model ensemble simulation in the LDAS for the current 6-hour analysis period. As part of this simulation, the LDAS assimilates the available SMAP observations and produces land analysis increments in two 3-hourly land analysis steps. The AGCM simulation during the Corrector segment is then forced with these land increments as well as the atmospheric tendency terms derived from the atmospheric analysis.

C. Experiment Design

A suite of three data assimilation experiments, summarized in Table I, was carried out to determine the impact of SMAP Tb assimilation on the skill of the simulated soil moisture and near-surface atmospheric variables. The control experiment (ADAS) assimilates the full stream of atmospheric observations as in FP operations, albeit in the coarser-resolution, 3D-Var ADAS configuration described above (section II-B). The ADAS experiment does not assimilate SMAP Tb. The second experiment (LADAS) is like the ADAS control experiment but with the additional assimilation of SMAP Tb observations in the weakly coupled LADAS configuration (section II-B). The LADAS experiment includes two-way feedback between the assimilation of SMAP Tb observations at the land surface and the atmospheric model and analysis. (Note that the ADAS control experiment is identical to running the LADAS without SMAP Tb assimilation because the only impact from the LDAS on the ADAS subsystem within the LADAS is through the soil moisture and temperature increments generated in the SMAP Tb analysis.) Finally, for reference we also conducted a land-only ("offline") assimilation experiment (LDAS$_{offl}$) that is forced with surface meteorological data from the Predictor segment of the ADAS control experiment and assimilates only SMAP Tb observations without feeding back on the atmospheric model or analysis.

The experiment period for the three data assimilation experiments is JJA 2017. To allow for spin-up, the AGCM in the ADAS control experiment was initialized on 1 April 2017 at 2100 UTC from MERRA-2 except for the land surface, which was initialized from a separate Catchment model simulation to address the structural land model changes between MERRA-2 and the recent GEOS version used here (section II-B). The latter, land-only, multi-decadal spin-up simulation consisted of a single member without perturbations and was driven with surface meteorological forcing data from

MERRA-2 through 2014 and from FP thereafter. The AGCM in the LADAS experiment was initialized from that of the ADAS control experiment on 3 May 2017 at 2100 UTC, allowing for a 4-week spin-up of the land analysis feedback. The 24-member land ensemble of the LDAS subsystem in the LADAS experiment was initialized from the LDAS ensemble Open Loop simulation (see section II-B), which was in turn initialized on 1 January 2015 at 0000 UTC from the above-mentioned land-only spin-up simulation. Finally, the LDAS$_{offl}$ experiment was initialized on 31 May 2017 at 2100 UTC from the LDAS ensemble in the LADAS experiment (Table I).

D. Data and Methods for Evaluation

This section describes the metrics and independent in situ measurements used to evaluate the output from the assimilation experiments. Depending on the variable, the performance metrics used here include the bias, unbiased root-mean-square error (ubRMSE, or standard deviation of the error) [57] and correlation (R) vs. the in situ measurements. We also estimate 95% confidence intervals for soil moisture correlation and ubRMSE following [28]. Estimates of soil moisture bias computed from point-scale in situ measurements are dominated by the large and unavoidable systematic errors in spatial upscaling, even for the locally dense SMAP core validation sites described below [58]. Hence, statistical confidence intervals are not shown for soil moisture bias estimates, and the differences in soil moisture bias estimates seen below are not considered statistically significant.

The in situ soil moisture measurements used here fall into two categories: (i) SMAP core validation sites with locally dense sensor networks that provide in situ measurements at the scale of the satellite measurements and model estimates [59]-[74] and (ii) so-called sparse networks with typically just one or two point-scale sensor profiles per satellite footprint, including the USDA Natural Resources Conservation Service Soil Climate Analysis Network (SCAN) [75], the U.S. Climate Reference Network (USCRN) [76], [77], the Oklahoma Mesonet [78], the SMOSMANIA network in the southwest of France [79], and the OzNet network in Australia [80].

Here, we use upscaled (33-km) surface (root-zone) soil moisture measurements for 12 (6) core sites. The sites match those in Table 1 of [81], except here we do *not* use surface measurements from Reynolds Creek, Ngari, St Josephs, Tonzi Ranch, Niger and Benin or root-zone measurements from Yanco for lack of sufficient in situ data during the JJA 2017 experiment period. Processing of the core site measurements follows [27]. The simulated soil moisture values are mapped to the core site locations using nearest-neighbor interpolation. Surface (root-zone) soil moisture measurements were available and used here from 360 (228) sparse network sites, which were grouped into 108 (76) clusters for the purpose of computing average metrics (for details, see section 6.3 and Table 2 of [81]). The in situ soil moisture measurements provide invaluable information but are subject to measurement errors and offer very limited coverage outside of the contiguous United States.

Following DR19, the simulated screen-level (2-m) specific

humidity (q2m) and air temperature (T2m) are evaluated vs. in situ measurements collated by the Hadley Centre Integrated Surface Database (HadISD version 3.1.1.202007p) [82], [83] and the Global Historical Climatology Network (GHCN; GHCN-DAILY version 3.26) [84], respectively. HadISD provides sub-daily (between hourly and 6-hourly), station-based, quality-controlled q2m data from ~7,000 stations during JJA 2017. GHCN provides station-based, quality-controlled measurements of daily maximum T2m ($T2m_{max}$) from ~12,000 stations. The stations in HadISD and GHCN are unevenly distributed across the globe, with good coverage in much of North America and Eurasia but generally poor coverage in the high latitudes, South America, Africa, the Tibetan Plateau, and central Australia (not shown). The AGCM-simulated q2m and T2m are diagnosed (interpolated) from the corresponding values at the surface and in the lowest atmospheric model layer using stability functions. The simulated q2m is written out at hourly intervals, mapped to each station location using a nearest-neighbor approach, and compared to the HadISD q2m whenever an observation is available. For each day and model grid cell, the simulated $T2m_{max}$ is determined from hourly AGCM output and mapped from the model grid to the GHCN station location using a nearest-neighbor approach. To improve the clarity of the illustrations, the metrics from the individual stations are averaged and plotted on a 2-degree latitude-longitude grid.

The 6-hour AGCM forecasts that provide the model background state during each assimilation cycle (section II-B; see Fig. 1 of DR19 for a schematic diagram) contain crucial information about the cumulative impact of the observations that were assimilated in all preceding cycles. Ideally, these forecasts match – within the assumed (that is, prescribed) model and observation error statistics – the corresponding observations, which have not yet been assimilated. The forecasts should be unbiased, and more accurate forecasts generally indicate a higher-quality analysis. We therefore examine key statistics of the observation-minus-forecast (OmF) residuals for the simulated L-band land surface Tb and atmospheric profiles of air temperature and humidity, including their mean, root-mean-square (RMS), and standard deviation. The OmF statistics for the L-band Tb are computed using SMAP Tb observations (after the climatological adjustment applied prior to assimilation; section II-B). The OmF statistics for air temperature and humidity profiles are computed against 6-hourly radiosonde observations at 6 vertical levels between 1000 and 300 mb from 397 locations over continental land, which we obtained from the NOAA Meteorological Assimilation Data Ingest System (http://madis.ncep.noaa.gov).

III. RESULTS AND DISCUSSION

A. Tb Residuals and Soil Moisture Increments

The LDAS subsystem in the LADAS is designed to minimize the disagreement between the SMAP-observed and model-simulated Tb. The proper functioning of the LDAS in its land-only configuration was thoroughly verified during repeated validation of the L4_SM product [27]-[29], [51]. Since here the

LDAS is used within the coupled LADAS, at a different resolution, and in the Catchment model's cube-sphere tile space (section II-B), this section confirms the proper functioning of the LDAS subsystem by briefly examining the Tb residuals and the resulting soil moisture analysis increments.

Fig. 1 shows the daily global mean and RMS of the Tb OmF residuals from the LADAS, along with the same for the Tb observation-minus-analysis (OmA) residuals. Whereas OmF residuals provide independent verification of the model forecast Tb (section II-D), OmA residuals are computed by differencing a SMAP Tb observation and a model forecast that was informed by this very observation. The daily variations in the OmF and OmA statistics are primarily caused by seasonal and weather-driven changes in land surface conditions. The daily coverage changes stemming from SMAP's 8-day exact repeat orbit play only a minor role. Across the experiment period, the daily mean Tb OmF and OmA values (cyan and orange bars, respectively) typically range from -0.5 to 0.5 K, with time series averages of -0.11 K for the OmF and -0.08 K for the OmA residuals (Fig. 1). The small magnitude of the mean Tb OmF residuals confirms that the Tb analysis largely free of bias, which is primarily a consequence of the climatological adjustment of the SMAP Tb observations prior to their assimilation (section II-B).

The daily global RMS of the Tb OmF residuals (blue bars in Fig. 1) ranges from 5 to 7.5 K, with a time series average (computed in quadrature) of 6.0 K. These values measure the typical misfit between a SMAP Tb observation and the corresponding model forecast for a given time and location. Finally, the daily RMS of the Tb OmA residuals (red bars) ranges from 3.5 to 4.5 K, with a time series average of 4.1 K; the reduction by ~2 K from the Tb OmF RMS is the result of the Tb analysis, which by design brings the model estimate closer to the assimilated observation. The OmF and OmA statistics seen here are fully consistent with those of the SMAP L4_SM algorithm [28]. This finding provides confidence in the proper workings of the LDAS subsystem in the cube-sphere tile space employed here (as opposed to the 9-km EASEv2 grid setup of the L4_SM algorithm).

Next, Fig. 2 illustrates the monthly mean of the analysis increments for the total profile soil moisture in equivalent flux units (mm d^{-1}), separately for June, July, and August 2017. The 3-hourly soil moisture increments underpinning the graphic were computed by the LDAS subsystem and then applied to the AGCM's land surface states in the ADAS subsystem of the LADAS. Owing to the nearly bias-free Tb analysis (Fig. 1), the soil moisture increments mostly vanish when averaged across longer periods [28]. For individual months, however, the monthly mean soil moisture increments typically range from -1.5 to 1.5 mm d^{-1}. For example, in June 2017 there is a strong negative (drying) increment in the center of the continental US (Fig. 2(a)), whereas in August 2017 the same region experiences a strong positive (wetting) increment (Fig. 2(c)). Compared to the monthly mean soil moisture increments of DR19 (their Fig. 5) for summer 2013, the increments seen here are more variable in space and time. This is primarily a consequence of the different bias correction strategies. DR19

assimilated soil moisture retrievals after cumulative distribution function matching [37]. Their approach does not remove seasonally-varying bias, which, if present, can dominate the signal in the soil moisture increments. Here, this mean seasonal bias is removed and only the anomaly signal in the SMAP Tb observations is assimilated (section II-B).

Finally, Fig. 3 shows the standard deviation of the surface soil moisture analysis increments, which measures the typical 3-hourly correction in the 0-5 cm surface layer resulting from a SMAP Tb analysis. (The statistic excludes increments that are trivially zero because at the time and location there was not a SMAP overpass within the ~1.25-degree radius of influence, or because the SMAP Tb observation did not pass quality control [51].) Regions with larger typical increments tend to be in the transition zones between wet and dry climates, including central North America, the Sahel, central Eurasia, and India (Fig. 3). These regions also coincide with croplands (e.g., Fig. A2.2 of [85]), where agricultural practices such as tilling, harvesting, or irrigation impact the SMAP Tb observations but are not represented in the LDAS modeling system, which can result in large Tb OmF values and, ultimately, large soil moisture increments (even though some systematic errors are removed through the climatological rescaling of the Tb observations prior to their assimilation into the land surface model; section II-B). Like the Tb OmF statistics, the spatial pattern and typical magnitudes of the increments standard deviation are consistent with those seen in the L4_SM algorithm [28] (their Fig. 7c). But the pattern is different from that seen for profile soil moisture increments in DR19 (their Fig. 5), which were relatively large throughout the high latitudes. The likely reason for the difference in the patterns is the aforementioned difference in the bias correction strategy applied prior to assimilation in DR19's retrieval assimilation.

B. Evaluation Using In Situ Measurements

Fig. 4 illustrates, for a representative location, the impact of the SMAP Tb assimilation on the quality of the simulated soil moisture and q2m in the LADAS experiment. During the JJA 2017 experiment period, the error in the ADAS-simulated (control) surface soil moisture vs. in situ measurements from the Waurika (WAUR) station in the Oklahoma Mesonet ranges from -0.15 to 0.1 m^3 m^{-3}, with a bias of -0.065 m^3 m^{-3} and an ubRMSE of 0.055 m^3 m^{-3} (Fig. 4(a)). (Note that the point-scale measurements provided by the station are not necessarily representative of the simulated grid-cell scale time average conditions.) The SMAP Tb assimilation in the LADAS reduces the surface soil moisture error by ~30%, resulting in a bias of -0.043 m^3 m^{-3} and an ubRMSE of 0.040 m^3 m^{-3} for the LADAS. The improvements extend to the simulated q2m (Fig. 4(b)); at a nearby HadISD station (#723510), the q2m bias is reduced from -0.91 g kg^{-1} in the ADAS control to -0.48 g kg^{-1} in the LADAS, and the q2m ubRMSE is slightly reduced from 1.53 g kg^{-1} in the ADAS control to 1.48 g kg^{-1} in the LADAS. There is good temporal consistency in the soil moisture and q2m improvements; errors in both variables are most reduced during the first half of July and in the second half of August.

1) Evaluation of Soil Moisture

The errors shown in Fig. 4 are just a representative example for a single location. Next, we examine the correlation, ubRMSE, and bias of the simulated, 3-hourly soil moisture when averaged across the sparse network sites and (separately) the core validation sites (Fig. 5). LADAS correlation skills for surface and root-zone soil moisture are ~0.5 at the sparse network sites and ~0.7-0.8 at the core sites (Fig. 5(a),(d)). At the sparse network sites, the correlation skill of surface and root-zone soil moisture in the LADAS exceeds that of the ADAS control by ~0.1. The skill increase is even larger at the core sites, with the LADAS correlation exceeding that of the ADAS control by 0.17 for surface and 0.26 for root-zone soil moisture. Because the estimated 95% confidence intervals do not overlap, the surface soil moisture skill improvements in the LADAS can be considered statistically significant, despite the relatively small sample size (owing to the short record and few stations available for validation).

The ubRMSE of the LADAS surface (root-zone) soil moisture is 0.043 (0.024) m^3 m^{-3} at the sparse network sites and 0.034 (0.022) m^3 m^{-3} at the core sites (Fig. 5(b),(e)). The LADAS ubRMSE values are all smaller than those of the ADAS control. Whereas the ubRMSE reductions are small (0.002-0.008 m^3 m^{-3}) and not statistically significant, they are consistent across surface and root-zone soil moisture and for the sparse network and core validation sites. The LADAS soil moisture is generally wetter than indicated by the in situ measurements, with an average bias in the surface (root-zone) soil moisture of 0.041 (0.027) m^3 m^{-3} at the sparse network sites and 0.021 (0.039) m^3 m^{-3} at the core sites (Fig. 5(c),(f)). Compared to the ADAS control, the LADAS bias is improved for surface soil moisture but degraded for root-zone soil moisture, consistently for sparse network and core validation sites. The generally larger soil moisture bias seen here (compared to that of the L4_SM product) is mainly because the land model precipitation forcing here is not corrected with gauge-based data. For root-zone soil moisture, the bias even exceeds the random error component (i.e., the ubRMSE).

2) Evaluation of Screen-Level Humidity and Temperature

Recall that the only difference between the ADAS subsystem within the weakly-coupled LADAS and the stand-alone ADAS is the additional forcing of the AGCM during the Corrector segment with the soil moisture increments generated by the SMAP Tb analysis in the LDAS subsystem (section II-B). That is, the SMAP Tb analysis impacts the simulated q2m and T2m primarily through the land-surface interactions encoded in the AGCM; the LDAS does not generate q2m or T2m increments, nor are q2m and T2m measurements assimilated in the ADAS control or LADAS. Consequently, we can use q2m and T2m measurements for an independent assessment of the quality of the simulated q2m and T2m and thereby determine the impact of SMAP Tb assimilation on the simulated screen-level estimates.

Fig. 6 shows the RMSE, bias, and ubRMSE of the ADAS-simulated (control) q2m vs. HadISD measurements in the left column and the difference between the LADAS and ADAS

control metrics in the right column. (For the bias, the difference is computed after taking the absolute value, to determine which bias is smaller in magnitude, independent of the sign of the bias.) The RMSE of the q2m estimates from the ADAS control experiment typically ranges between 1 and 3 g kg^{-1}, with values exceeding 2.5 g kg^{-1} in some regions, somewhat lower values in the Southern Hemisphere mid-latitudes, and a global land average RMSE of 1.70 g kg^{-1} (Fig. 6(a)). The ADAS-simulated q2m is generally too moist by ~0.5-1 g kg^{-1} in the higher latitudes and too dry by ~1-2 g kg^{-1} in the Subtropics and Tropics, with a global average dry bias of -0.38 g kg^{-1} (Fig. 6(c)). Consequently, the q2m ubRMSE values are only somewhat smaller than the RMSE values, with a global average of 1.38 g kg^{-1} (Fig. 6(e)).

Overall, the assimilation of SMAP Tb in the LADAS improves the q2m estimates compared to those of the ADAS control. The q2m RMSE is considerably improved by ~0.3 g kg^{-1} in the Northern Great Plains (incl. Canadian Plains), the western Sahel, and northern India along the Himalayas (Fig. 6(b)). Smaller improvements are seen across much of central Eurasia, and only a few small areas show a degradation in the LADAS q2m RMSE, including a slight degradation in the southeastern United States. In the global land average, the q2m RMSE is slightly reduced by 0.05 g kg^{-1}. Much of the q2m RMSE improvement is from a reduction in the (absolute) bias, especially in central Eurasia and Eastern Europe, although some increase in the absolute bias is seen in smaller regions scattered across the globe (Fig. 6(d)). In contrast, the q2m ubRMSE shows a smaller improvement across the globe, particularly in the regions where the RMSE is improved the most, including the Northern Great Plains (incl. Canadian Plains), northern India, and central Eurasia (Fig. 6(f)). Like the q2m RMSE, the ubRMSE improvement is very consistent; there is almost no degradation in the LADAS statistic seen anywhere across the globe.

Next, Fig. 7 illustrates the impact of the SMAP Tb assimilation on T2m$_{max}$; the figure again shows the ADAS control metrics in the left column and the LADAS minus ADAS differences in the metrics in the right column. The T2m$_{max}$ RMSE for the ADAS ranges from ~1-2 K in much of Europe and Australia to ~3.5 K elsewhere, with a global average of 2.77 K (Fig. 7(a)). The ADAS T2m$_{max}$ estimates are too cold by 0.7 K on average; they are too cold by ~2 K at the majority of the GHCN stations but too warm 1-2 K in some regions, including the southwestern US and the western Sahel (Fig. 7(b)). The T2m$_{max}$ ubRMSE is 1.77 K on average and ranges between 0.5 and 1.5 K in much of Europe and Australia and between 1.5 and 3 K in the Americas and Africa (Fig. 7(c)).

On average, the T2m$_{max}$ RMSE in the LADAS is slightly improved compared to that of the ADAS control, by 0.04 K. The largest RMSE reductions of up to 0.4 K, or ~20% of the RMSE, are seen in the central US, the western Sahel, across several subregions of Eurasia, and in central Australia; but there is also some degradation, most notably in Argentina (Fig. 7(b)). The net improvement in the (absolute) bias is 0.02 K on average, with a spatial pattern of change like that seen for the RMSE. The ubRMSE in the LADAS is reduced from that of the

ADAS control by 0.03 K on average, with improvements of up to ~0.3 K in the above-mentioned regions that showed noteworthy RMSE reductions. The T2m$_{max}$ ubRMSE improvement is also very consistent across the globe; there is only some scattered degradation, typically by less than 0.2 K. Moreover, the improvements in the LADAS T2m$_{max}$ estimates are consistent with those in q2m, as evidenced by their very similar spatial pattern (compare the metrics difference plots of Figs. 6 and 7). This pattern is also consistent with that of the typical magnitude of the soil moisture increments (Fig. 2).

The q2m and T2m skill metrics (Figs. 6 and 7) seen here are comparable to those of DR19 for mid-April through August of 2013 (their Figs. 9 and 10), with generally consistent spatial patterns. This suggests that the improved modeling system used here at least partly compensates for not using the gauge-based precipitation corrections employed in DR19. Moreover, the improvements in the LADAS q2m and T2m$_{max}$ estimates seen here are also comparable in magnitude to those of DR19 for their ASCAT and SMOS retrieval assimilation. In both studies, the bias improvements contribute more to the RMSE reduction than do the ubRMSE improvements. However, the LADAS improvements seen here include fewer regions of degraded skill and are overall more coherent than those of DR19. Possible reasons for this include the two studies' differences in the bias correction method applied prior to assimilation, the spatially distributed vs. local soil moisture analysis approach, and the generally better soil moisture information provided by the SMAP Tb observations compared to that of the ASCAT and SMOS retrievals.

C. Impact on Atmospheric Background States

In this section, we investigate the impact of the SMAP Tb analysis on the atmospheric background forecast in the ADAS subsystem of the LADAS. The black dots in Fig. 8 show vertical profiles of the JJA 2017 mean and standard deviation of specific humidity and air temperature OmF residuals from the ADAS control experiment, computed using radiosonde observations over continental land only. On average, the ADAS background forecast is too dry by 0.2 g kg^{-1} at the surface (Fig. 8(a)), which is consistent with the q2m station comparison of Fig. 6(c). In the lower and middle troposphere, however, the ADAS specific humidity is too moist by 0.1 g kg^{-1} (Fig. 8(a)). There is also a cold bias in the ADAS air temperature of ~0.3 K at the 850-1000 mb levels (Fig. 8(c)), which is consistent with the screen-level T2m$_{max}$ being too cold on average (Fig. 7(c)). The OmF standard deviation for specific humidity is ~1.5 g kg^{-1} below 500 mb (Fig. 8(b)), and the OmF standard deviation for air temperature ranges from nearly 2 K close to the surface to ~1 K through the mid-troposphere (Fig. 8(d)).

The blue bars in Fig. 8 indicate the relative skill differences in percentage units between the LADAS and ADAS statistics, with negative values indicating that the (absolute) mean or standard deviation of the LADAS OmF is reduced (improved) from that of the ADAS control experiment and positive values indicating degradation. For specific humidity estimates from the LADAS, the OmF (absolute) mean is improved by 15-25% and the standard deviation is improved slightly by 1-2% in the

lower troposphere (Fig. 8(a),(b)), with a largely neutral impact in the mid-troposphere. Near the surface (850-1000 mb), this translates into an improvement of ~0.02-0.03 g kg^{-1} in the (absolute) mean and an improvement of ~0.01-0.02 g kg^{-1} in the standard deviation, which is consistent with that seen in the evaluation against screen-level measurements (Fig. 6). In contrast, air temperature estimates from the LADAS show a small degradation (increase) of 2-3% in the (absolute) bias and a slight improvement of ~0.5% in the standard deviation in the lower troposphere, but both relative differences translate into minimal changes of less than 0.01 K. Similarly, the ~10% improvement in the LADAS air temperature bias from that of the ADAS control at 400-500 mb is minimal (less than 0.01 K) and, given the mixed results in the lower tropospheric temperature, this nominal improvement is most likely noise and not related to the SMAP Tb analysis. In summary, the impact of the SMAP Tb analysis on the atmospheric background forecasts in the LADAS is, as expected, most prominent and beneficial for specific humidity near the surface and mostly neutral in the mid-troposphere.

D. Weakly Coupled vs. Stand-alone Land Analysis

The positive impact of the SMAP Tb analysis on soil moisture, q2m, and T2m$_{max}$ seen above may also improve the quality of the land surface meteorological forcing data in the LADAS, including precipitation, radiation, air temperature, humidity, and wind in the lowest model layer of the AGCM. The improved forcing data may then, in turn, result in improved Tb background forecasts in the LDAS subsystem of the LADAS. Since the latter is forced with data from the AGCM's Predictor segment in the LADAS, the supplemental, land-only LDAS experiment (LDAS$_{offl}$) was driven with surface meteorological forcing data from the Predictor segment of the ADAS control experiment (section II-B, Table I). If the SMAP Tb analysis does indeed improve the surface meteorological forcing data in the LADAS, the typical magnitude of the Tb OmF residuals in its LDAS subsystem should be smaller than that of the Tb OmF residuals in the LDAS$_{offl}$ experiment. This expectation is confirmed in Fig. 9, which shows a mostly negative difference in the RMS of the Tb OmF residuals between the LADAS and LDAS$_{offl}$ experiments. The difference is very small during June 2017 but generally increases during the experiment period, which suggests that the LADAS may still be spinning up during much of the JJA experiment period. By August 2017, the typical Tb OmF residuals from the LADAS are smaller by up to ~0.1 K than those from LDAS$_{offl}$. This difference is comparable to the reduction in the Tb OmF RMS achieved with the Catchment model improvements introduced with Version 4 of the L4_SM product [28].

The improvements seen in Fig. 9 indicate that it is beneficial to conduct the SMAP Tb analysis in the weakly coupled system, permitting feedback from the improved soil moisture estimates on the surface meteorological forcing data, which in turn improves the land surface analysis beyond what is possible with "fixed" forcing from an entirely separate ADAS. Further indication of the improvements associated with this coupling is seen in Fig. 5, which includes skill metrics for the LDAS$_{offl}$

experiment in addition to those of the ADAS control and LADAS experiments that were discussed above (section III-B). Whereas the skill differences between the LADAS and LDAS$_{offl}$ soil moisture estimates are very small and not statistically significant, the surface and root-zone soil moisture ubRMSE for LADAS is slightly but consistently better than that of the LDAS$_{offl}$ experiment for both the core validation and sparse network sites (Fig. 5(b),(e)). Compared to LDAS$_{offl}$, the LADAS also has somewhat better root-zone soil moisture correlation skill at the core sites (Fig. 5(d)) and lower bias at the sparse network sites (Fig. 5(c),(f)), although the LADAS has slightly worse correlation at the sparse network sites (Fig. 5(a),(d)) and slightly worse bias at the core sites (Fig. 5(c),(f)). The relatively small magnitude of the differences between the LADAS and LDAS$_{offl}$ metrics are consistent with the multi-step nature of the soil moisture feedback on the atmospheric forcing [86].

IV.   SUMMARY AND CONCLUSION

SMAP has been providing L-band microwave brightness temperature observations of unprecedented quality that are highly sensitive to surface soil moisture unless the soil is frozen or obscured by dense vegetation. This study's main objective is to examine the impact of assimilating SMAP Tb observations in a weakly-coupled land-atmosphere data assimilation system. To this end, we use the recently developed GEOS LADAS, which couples the SMAP Tb analysis from the land-only L4_SM algorithm with the GEOS ADAS used for weather analysis. We use the latter in 3D-Var configuration as in MERRA-2, but with the model and atmospheric analysis improvements implemented since MERRA-2. By comparing the LADAS results to those from stand-alone ADAS and LDAS$_{offl}$ experiments, we demonstrate that the SMAP Tb analysis improves the LADAS-simulated soil moisture, screen-level atmospheric variables, and near-surface atmospheric humidity and temperature profiles.

Specifically, we find that the SMAP Tb analysis in the LDAS subsystem of the LADAS yields statistics of the Tb OmF residuals and soil moisture analysis increments like those generated by the well-tested, land-only L4_SM algorithm (Figs. 1-3), which confirms the proper functioning of the LDAS subsystem, especially its setup in the cube-sphere tile space used here and its coupling to ADAS subsystem.

Validation vs. in situ measurements of surface and root-zone soil moisture, q2m, and T2m$_{max}$ demonstrates the beneficial impact of the SMAP Tb analysis in the LADAS. LADAS-simulated surface and root-zone soil moisture has higher correlation and lower ubRMSE than corresponding ADAS control estimates when validated against in situ measurements from 12 SMAP core sites and 360 stations across five sparse networks (Fig. 5). The benefit of the SMAP Tb analysis seen here is fully consistent with prior validation results of the L4_SM product [28]-[29]. We further show that LADAS-simulated q2m and T2m$_{max}$ have, on average, slightly lower RMSE, ubRMSE, and (absolute) bias than corresponding ADAS control estimates (Fig. 6-7). There are very few instances of degraded performance, and RMSE values are

improved by up to 0.3 g kg^{-1} for q2m and up to 0.4 K for T2m$_{max}$ in some regions. Improvements are relatively larger in q2m than T2m$_{max}$, which is consistent with the fact that SMAP primarily provides information about the water cycle. The smaller improvements in LADAS screen-level temperature and humidity estimates compared to those in soil moisture estimates are consistent with the fact that soil moisture is only one factor determining T2m and q2m. Errors in the model parameterization of the coupling between soil moisture and screen-level parameters, for example, are not corrected through the assimilation of SMAP Tb measurements.

An examination of the OmF residuals for Tb (using SMAP observations) and atmospheric specific humidity and air temperature profiles (using radiosonde measurements) further illustrates that the benefit of the SMAP Tb analysis in the weakly coupled LADAS is not limited to soil moisture but also improves near-surface atmospheric humidity and temperature through the dynamic interactions between the land surface and the atmosphere (Figs. 8-9). This result is also confirmed by a comparison of the Tb OmF residuals and soil moisture skill metrics from the LADAS with those from the land-only LDAS$_{offl}$ experiment (Figs. 5 and 9), which indicate slightly better skill in the LADAS compared to LDAS$_{offl}$.

The results of this study are largely consistent with those of DR19, although it is difficult to compare their results to ours. DR19's experiment period in 2013 precedes the launch of SMAP. Moreover, DR19 used gauge-based precipitation corrections, which increase soil moisture simulation skill in well-observed regions such as the United States and Western Europe, although they have limited impact on skill across much of the globe [29]. Compared to the MERRA-2 baseline system of DR19, however, the present study used an improved version of the GEOS ADAS, making it harder for the SMAP Tb analysis to yield improvements. Nevertheless, the assimilation of SMAP Tb observations improved the LADAS-simulated soil moisture and near surface air humidity and temperature by at least as much as did the assimilation of ASCAT and SMOS soil moisture retrievals in DR19, presumably owing to (i) the higher quality of the assimilated SMAP data and (ii) the improved, spatially distributed, radiance-based Tb analysis of the L4_SM algorithm. A follow-up investigation of the separate and joint assimilation of ASCAT, SMOS, and SMAP observations in the current version of the LADAS promises to yield further insights but was beyond the scope of the present study, given the considerable computational demands of the LADAS.

The updated GEOS LADAS is therefore a promising tool for use in the near-real time GEOS FP weather analysis and future GEOS-based reanalysis products. Additional validation and development, however, is needed. For example, tower-based measurements of evapotranspiration and sensible heat fluxes were not yet publicly available in sufficient quantity for the JJA 2017 experiment period. Once such records become available, it is important to assess the impact of the SMAP Tb analysis on the quality of the simulated surface turbulent fluxes. Alternatively, evapotranspiration data derived from thermal infrared satellite observations could be used [87]. Moreover, the impact of the SMAP Tb analysis on medium-range weather forecasts (as opposed to the 6-hour atmospheric background forecasts that are part of the atmospheric analysis) needs to be assessed.

Finally, the weakly-coupled LADAS needs to be tested in the context of the quasi-operational, near-real time, 12.5-km resolution GEOS FP weather analysis, which uses a hybrid 4-dimensional ensemble variational (Hybrid 4D-EnVar) approach [88]. Preliminary results (not shown) derived using a prototype LADAS version based on the Hybrid 4D-EnVar ADAS are encouraging, but more development is needed. The coupling of the ensemble-based LDAS subsystem to the ensemble-based atmospheric analysis involves a slew of design choices and opportunities. First, having access to an *ensemble* of surface meteorological forcing data from the Hybrid 4D-EnVar should provide a more realistic representation of uncertainty in the surface meteorological forcing of the land than do the purely statistical perturbations used heretofore in the LDAS [89]. Second, the ensemble of land increments can be fed back into the ensemble of AGCM simulations of the Hybrid 4D-EnVar ADAS (rather than feeding only the ensemble-average LDAS increments back into the ADAS). Clearly, continued development of the LADAS is needed to further constrain errors in soil moisture and near-surface atmospheric variables, thereby improving analysis estimates and medium-range forecasts of T2m, q2m, surface fluxes, and land surface conditions. More generally, the weakly coupled LADAS presented here is just one small step towards the community's ultimate objective of a fully coupled Earth system analysis.

REFERENCES

[1] R. D. Koster, P.A. Dirmeyer, Z. Guo, G. Bonan, E. Chan, P. Cox, C.T. Gordon, S. Kanae, E. Kowalczyk, D. Lawrence, P. Liu, C.-H. Lu, S. Malyshev, B. McAvaney, K. Mitchell, D. Mocko, T. Oki, K. Oleson, A. Pitman, Y.C. Sud, C.M. Taylor, D. Verseghy, R. Vasic, Y. Xue, and T. Yamada, "Regions of Strong Coupling Between Soil Moisture and Precipitation," *Science*, vol. 305, no. 5687, pp. 1138–1140, Aug. 2004.

[2] S. I. Seneviratne, T. Corti, E. L. Davin, M. Hirschi, E. B. Jaeger, I. Lehner, B. Orlowsky, and A. J. Teuling, "Investigating soil moisture–climate interactions in a changing climate: A review," *Earth-Science Reviews*, vol. 99, no. 3–4, pp. 125–161, May 2010.

[3] R. D. Koster, S. P. P. Mahanama, T. J. Yamada, G. Balsamo, A. A. Berg, M. Boisserie, P. A. Dirmeyer, F. J. Doblas-Reyes, G. Drewitt, C. T. Gordon, Z. Guo, J.-H. Jeong, W.-S. Lee, Z. Li, L. Luo, S. Malyshev, W. J. Merryfield, S. I. Seneviratne, T. Stanelle, B. J. J. M. van den Hurk, F. Vitart, and E. F. Wood, "The Second Phase of the Global Land–Atmosphere Coupling Experiment: Soil Moisture Contributions to Subseasonal Forecast Skill," *Journal of Hydrometeorology*, vol. 12, no. 5, pp. 805–822, Oct. 2011.

[4] S. Tuttle and G. Salvucci, "Empirical evidence of contrasting soil moisture-precipitation feedbacks across the United States," *Science*, vol. 352, no. 6287, pp. 825–828, May 2016.

[5] J. A. Santanello, P. A. Dirmeyer, C. R. Ferguson, K. L. Findell, A. B. Tawfik, A. Berg, M. Ek, P. Gentine, B. P. Guillod, C. van Heerwaarden, J. Roundy, and V. Wulfmeyer, "Land–Atmosphere Interactions: The LoCo Perspective," *Bulletin of the American Meteorological Society*, vol. 99, no. 6, pp. 1253–1272, Jun. 2018.

[6] P. A. Levine, J. T. Randerson, S. C. Swenson, and D. M. Lawrence, "Evaluating the strength of the land–atmosphere moisture feedback in Earth system models using satellite observations," *Hydrology and Earth System Sciences*, vol. 20, no. 12, pp. 4837–4856, Dec. 2016.

[7] R. H. Reichle, "Data assimilation methods in the Earth sciences," *Advances in Water Resources*, vol. 31, no. 11, pp. 1411–1418, Nov. 2008.

[8] J.-F. Mahfouf, "Analysis of Soil Moisture from Near-Surface Parameters: A Feasibility Study," *Journal of Applied Meteorology*, vol. 30, no. 11, pp. 1534–1547, Nov. 1991.

[9] R. Hess, "Assimilation of screen-level observations by variational soil moisture analysis," *Meteorology and Atmospheric Physics*, vol. 77, no. 1–4, pp. 145–154, Sep. 2001.

[10] S. Bélair, L.-P. Crevier, J. Mailhot, B. Bilodeau, and Y. Delage, "Operational Implementation of the ISBA Land Surface Scheme in the Canadian Regional Weather Forecast Model. Part I: Warm Season Results," *Journal of Hydrometeorology*, vol. 4, no. 2, pp. 352–370, Apr. 2003.

[11] M. Drusch and P. Viterbo, "Assimilation of Screen-Level Variables in ECMWF's Integrated Forecast System: A Study on the Impact on the Forecast Quality and Analyzed Soil Moisture," *Monthly Weather Review*, vol. 135, no. 2, pp. 300–314, Feb. 2007.

[12] I. Dharssi, K. J. Bovis, B. Macpherson, and C. P. Jones, "Operational assimilation of ASCAT surface soil wetness at the Met Office," *Hydrology and Earth System Sciences*, vol. 15, no. 8, pp. 2729–2746, Aug. 2011.

[13] P. de Rosnay, M. Drusch, D. Vasiljevic, G. Balsamo, C. Albergel, and L. Isaksen, "A simplified Extended Kalman Filter for the global operational soil moisture analysis at ECMWF," *Quarterly Journal of the Royal Meteorological Society*, vol. 139, no. 674, pp. 1199–1213, Sep. 2012.

[14] S. G. Benjamin, S. S. Weygandt, J. M. Brown, M. Hu, C. R. Alexander, T. G. Smirnova, J. B. Olson, E. P. James, D. C. Dowell, G. A. Grell, H. Lin, S. E. Peckham, T. L. Smith, W. R. Moninger, J. S. Kenyon, and G. S. Manikin, "A North American Hourly Assimilation and Model Forecast Cycle: The Rapid Refresh," *Monthly Weather Review*, vol. 144, no. 4, pp. 1669–1694, Apr. 2016.

[15] J. A. Milbrandt, S. Bélair, M. Faucher, M. Vallée, M. L. Carrera, and A. Glazer, "The Pan-Canadian High Resolution (2.5 km) Deterministic Prediction System," *Weather and Forecasting*, vol. 31, no. 6, pp. 1791–1816, Nov. 2016.

[16] M. L. Carrera, B. Bilodeau, S. Bélair, M. Abrahamowicz, A. Russell, and X. Wang, "Assimilation of Passive L-band Microwave Brightness Temperatures in the Canadian Land Data Assimilation System: Impacts on Short-Range Warm Season Numerical Weather Prediction," *Journal of Hydrometeorology*, vol. 20, no. 6, pp. 1053–1079, May 2019.

[17] V. Naeimi, K. Scipal, Z. Bartalis, S. Hasenauer, and W. Wagner, "An Improved Soil Moisture Retrieval Algorithm for ERS and METOP Scatterometer Observations," *IEEE Transactions on Geoscience and Remote Sensing*, vol. 47, no. 7, pp. 1999–2013, Jul. 2009.

[18] W. Wagner, S. Hahn, R. Kidd, T. Melzer, Z. Bartalis, S. Hasenauer, J. Figa-Saldaña, P. de Rosnay, A. Jann, S. Schneider, J. Komma, G. Kubu, K. Brugger, C. Aubrecht, J. Züger, U. Gangkofner, S. Kienberger, L. Brocca, Y. Wang, G. Blöschl, J. Eitzinger, and K. Steinnocher, "The ASCAT Soil Moisture Product: A Review of its Specifications, Validation Results, and Emerging Applications," *Meteorologische Zeitschrift*, vol. 22, no. 1, pp. 5–33, Feb. 2013.

[19] Y. H. Kerr, P. Waldteufel, J.-P. Wigneron, S. Delwart, F. Cabot, J. Boutin, M.-J. Escorihuela, J. Font, N. Reul, C. Gruhier, S. E. Juglea, M. R. Drinkwater, A. Hahne, M. Martín-Neira, and S. Mecklenburg, "The SMOS Mission: New Tool for Monitoring Key Elements of the Global Water Cycle," *Proceedings of the IEEE*, vol. 98, no. 5, pp. 666–687, May 2010.

[20] Y. H. Kerr, A. Al-Yaari, N. Rodriguez-Fernandez, M. Parrens, B. Molero, D. Leroux, S. Bircher, A. Mahmoodi, A. Mialon, P. Richaume, S. Delwart, A. Al Bitar, T. Pellarin, R. Bindlish, T. J. Jackson, C. Rüdiger, P. Waldteufel, S. Mecklenburg, and J.-P. Wigneron, "Overview of SMOS performance in terms of global soil moisture monitoring after six years in operation," *Remote Sensing of Environment*, vol. 180, pp. 40–63, Jul. 2016.

[21] D. Entekhabi, E. G. Njoku, P. E. O'Neill, K. H. Kellogg, W. T. Crow, W. N. Edelstein, J. K. Entin, S. D. Goodman, T. J. Jackson, J. Johnson, J. Kimball, J. R. Piepmeier, R. D. Koster, N. Martin, K. C. McDonald, M. Moghaddam, S. Moran, R. Reichle, J. C. Shi, M. W. Spencer, S. W. Thurman, L. Tsang, and J. Van Zyl, "The Soil Moisture Active Passive (SMAP) Mission," *Proceedings of the IEEE*, vol. 98, no. 5, pp. 704–716, May 2010.

[22] S. K. Chan, R. Bindlish, P. E. O'Neill, E. Njoku, T. Jackson, A. Colliander, F. Chen, M. Burgin, S. Dunbar, J. Piepmeier, S. Yueh, D. Entekhabi, M. H. Cosh, T. Caldwell, J. Walker, X. Wu, A. Berg, T. Rowlandson, A. Pacheco, H. McNairn, M. Thibeault, J. Martinez-Fernandez, A. Gonzalez-Zamora, M. Seyfried, D. Bosch, P. Starks, D. Goodrich, J. Prueger, M. Palecki, E. E. Small, M. Zreda, J.-C. Calvet, W. T. Crow, and Y. Kerr, "Assessment of the SMAP Passive Soil Moisture Product," *IEEE Transactions on Geoscience and Remote Sensing*, vol. 54, no. 8, pp. 4994–5007, Aug. 2016.

[23] J. Muñoz-Sabater, H. Lawrence, C. Albergel, P. Rosnay, L. Isaksen, S. Mecklenburg, Y. Kerr, and M. Drusch, "Assimilation of SMOS brightness temperatures in the ECMWF Integrated Forecasting System," *Quarterly Journal of the Royal*

Meteorological Society, vol. 145, no. 723, pp. 2524–2548, Jul. 2019.

[24] ECMWF, "IFS Documentation CY46R1 - Part II: Data Assimilation," *ECMWF*, 2019, doi: 10.21957/D6FOT95HI.

[25] B. Gómez, C. L. Charlton-Pérez, H. Lewis, and B. Candy, "The Met Office Operational Soil Moisture Analysis System," *Remote Sensing*, vol. 12, no. 22, p. 3691, Nov. 2020.

[26] J. W. Wegiel, "Data Assimilation Enhancements to Air Force Weather's Land Information System," presented at 100th American Meteorological Society Annual Meeting, 34th Conference on Hydrology, Boston, MA, USA, Jan. 2020. [Online] Available: https://ams.confex.com/ams/2020Annual/webprogram/Paper366952.html

[27] R. H. Reichle, G. J. M. De Lannoy, Q. Liu, J. V. Ardizzone, A. Colliander, A. Conaty, W. Crow, T. J. Jackson, L. A. Jones, J. S. Kimball, R. D. Koster, S. P. Mahanama, E. B. Smith, A. Berg, S. Bircher, D. Bosch, T. G. Caldwell, M. Cosh, Á. González-Zamora, C. D. Holifield Collins, K. H. Jensen, S. Livingston, E. Lopez-Baeza, J. Martínez-Fernández, H. McNairn, M. Moghaddam, A. Pacheco, T. Pellarin, J. Prueger, T. Rowlandson, M. Seyfried, P. Starks, Z. Su, M. Thibeault, R. van der Velde, J. Walker, X. Wu, and Y. Zeng, "Assessment of the SMAP Level-4 Surface and Root-Zone Soil Moisture Product Using In Situ Measurements," *Journal of Hydrometeorology*, vol. 18, no. 10, pp. 2621–2645, Sep. 2017.

[28] R. H. Reichle, Q. Liu, R. D. Koster, W. T. Crow, G. J. M. De Lannoy, J. S. Kimball, J. V. Ardizzone, D. Bosch, A. Colliander, M. Cosh, J. Kolassa, S. P. Mahanama, J. Prueger, P. Starks, and J. P. Walker, "Version 4 of the SMAP Level-4 Soil Moisture Algorithm and Data Product," *Journal of Advances in Modeling Earth Systems*, vol. 11, no. 10, pp. 3106–3130, Oct. 2019.

[29] R. H. Reichle, Q. Liu, J. V. Ardizzone, W. T. Crow, G. J. M. De Lannoy, J. Dong, J. S. Kimball, and R. D. Koster, "The Contributions of Gauge-Based Precipitation and SMAP Brightness Temperature Observations to the Skill of the SMAP Level-4 Soil Moisture Product," *Journal of Hydrometeorology*, vol. 22, no. 2, pp. 405–424, Feb. 2021.

[30] R. Lucchesi, "File Specification for GEOS-5 FP (Forward Processing)", GMAO Office Note No. 4 (Version 1.2), 56pp, 2018. [Online]. Available: http://gmao.gsfc.nasa.gov/publications.

[31] R. Gelaro, W. McCarty, M. J. Suárez, R. Todling, A. Molod, L. Takacs, C. A. Randles, A. Darmenov, M. G. Bosilovich, R. Reichle, K. Wargan, L. Coy, R. Cullather, C. Draper, S. Akella, V. Buchard, A. Conaty, A. M. da Silva, W. Gu, G.-K. Kim, R. Koster, R. Lucchesi, D. Merkova, J. E. Nielsen, G. Partyka, S. Pawson, W. Putman, M. Rienecker, S. D. Schubert, M. Sienkiewicz, and B. Zhao, "The Modern-Era Retrospective Analysis for Research and Applications, Version 2 (MERRA-2)," *Journal of Climate*, vol. 30, no. 14, pp. 5419–5454, Jul. 2017.

[32] R. H. Reichle, Q. Liu, R. D. Koster, C. S. Draper, S. P. P. Mahanama, and G. S. Partyka, "Land Surface Precipitation in MERRA-2," *Journal of Climate*, vol. 30, no. 5, pp. 1643–1664, Feb. 2017.

[33] C. Draper and R. H. Reichle, "Assimilation of Satellite Soil Moisture for Improved Atmospheric Reanalyses," *Monthly Weather Review*, vol. 147, no. 6, pp. 2163–2188, Jun. 2019.

[34] S. V. Kumar, P. A. Dirmeyer, C. D. Peters-Lidard, R. Bindlish, and J. Bolten, "Information theoretic evaluation of satellite soil moisture retrievals," *Remote Sensing of Environment*, vol. 204, pp. 392–400, Jan. 2018.

[35] H. E. Beck, M. Pan, D. G. Miralles, R. H. Reichle, W. A. Dorigo, S. Hahn, J. Sheffield, L. Karthikeyan, G. Balsamo, R. M. Parinussa, A. I. J. M. van Dijk, J. Du, J. S. Kimball, N. Vergopolan, and E. F. Wood, "Evaluation of 18 satellite- and model-based soil moisture products using in situ measurements from 826 sensors," *Hydrology and Earth System Sciences*, vol. 25, no. 1, pp. 17–40, Jan. 2021.

[36] E. Seo, M.-I. Lee, and R. H. Reichle, "Assimilation of SMAP and ASCAT soil moisture retrievals into the JULES land surface model using the Local Ensemble Transform Kalman Filter," *Remote Sensing of Environment*, vol. 253, p. 112222, Feb. 2021.

[37] R. H. Reichle and R. D. Koster, "Bias reduction in short records of satellite soil moisture," *Geophysical Research Letters*, vol. 31, no. 19, 2004.

[38] G. J. M. De Lannoy and R. H. Reichle, "Assimilation of SMOS brightness temperatures or soil moisture retrievals into a land surface model," *Hydrology and Earth System Sciences*, vol. 20, no. 12, pp. 4895–4911, Dec. 2016.

[39] N. P. Arnold, W. M. Putman, and S. R. Freitas, "Impact of Resolution and Parameterized Convection on the Diurnal Cycle of Precipitation in a Global Nonhydrostatic Model," *Journal of the Meteorological Society of Japan*. Ser. II, vol. 98, no. 6, pp. 1279–1304, 2020.

[40] S. Chan, E. G. Njoku, and A. Colliander, "SMAP L1C Radiometer Half-Orbit 36 km EASE-Grid Brightness Temperatures, Version 4." *NASA National Snow and Ice Data Center DAAC*, 2018, doi: 10.5067/ZVILG0PS6CTI.

[41] M. J. Brodzik, B. Billingsley, T. Haran, B. Raup, and M. H. Savoie, "EASE-Grid 2.0: Incremental but Significant Improvements for Earth-Gridded Data Sets," *ISPRS International Journal of Geo-Information*, vol. 1, no. 1, pp. 32–45, Mar. 2012.

[42] M. M. Rienecker, M. J. Suarez, R. Gelaro, R. Todling, J. Bacmeister, E. Liu, M. G. Bosilovich, S. D. Schubert, L. Takacs, G.-K. Kim, S. Bloom, J. Chen, D. Collins, A. Conaty, A. da Silva, W. Gu, J. Joiner, R. D. Koster, R. Lucchesi, A. Molod, T. Owens, S. Pawson, P. Pegion, C. R. Redder, R. Reichle, F. R. Robertson, A. G. Ruddick, M. Sienkiewicz, and J. Woollen, "MERRA: NASA's Modern-Era Retrospective Analysis for Research and Applications," *Journal of Climate*, vol. 24, no. 14, pp. 3624–3648, Jul. 2011.

[43] R. D. Koster, R. H. Reichle, S. P. P. Mahanama, J. Perket, Q. Liu, and G. Partyka, "Land-Focused Changes in the Updated GEOS FP System (Version 5.25)", NASA Global Modeling and Assimilation Office Research Brief, 11 pp, Mar. 2020. [Online]. Available: https://gmao.gsfc.nasa.gov/researchbriefs/land_changes_GEOS-FP/land_changes_GEOS-FP.pdf.

[44] N. Arnold, W. Putman, S. Freitas, L. Takacs, and S. Rabenhorst, "Impacts of new atmospheric physics in the updated GEOS FP system (Version 5.25)", NASA Global Modeling and Assimilation Office Research Brief, 13 pp, Sep. 2020. [Online]. Available: https://gmao.gsfc.nasa.gov/researchbriefs/new_atmos_phys_GEOS-FP/new_atmos_phys_GEOS-FP.pdf.

[45] P. Norris, L. L. Takacs, W. Putman, L. Coy, S. Pawson, E. Mlawer, and M. Iacono,"Transition to the RRTMG Shortwave Radiation Code in GEOS Models", NASA Global Modeling and Assimilation Office Research Brief, 11 pp, Jun. 2020. [Online]. Available: https://gmao.gsfc.nasa.gov/researchbriefs/sw_rrtmg_transition/sw_rrtmg_transition.pdf.

[46] S. Akella, R. Todling, and M. Suarez, "Assimilation for skin SST in the NASA GEOS atmospheric data assimilation system," *Quarterly Journal of the Royal Meteorological Society*, vol. 143,

no. 703, pp. 1032–1046, Jan. 2017.

[47] W. Gu, R. Todling and D. N. Daescu, "Accounting for correlated satellite observation errors in GSI," presented at the Annual Meeting of the American Meteorological Society, Fifth AMS Symp. on the Joint Center for Satellite Data Assimilation, Seattle, WA, USA, 2017. [Online]. Available: https://ams.confex.com/ams/97Annual/webprogram/Paper307863.html.

[48] S. C. Bloom, L. L. Takacs, A. M. da Silva, and D. Ledvina, "Data Assimilation Using Incremental Analysis Updates," *Monthly Weather Review*, vol. 124, no. 6, pp. 1256–1271, Jun. 1996.

[49] L. L. Takacs, M. J. Suárez, and R. Todling, "The Stability of Incremental Analysis Update," *Monthly Weather Review*, vol. 146, no. 10, pp. 3259–3275, Sep. 2018.

[50] G. J. M. De Lannoy and R. H. Reichle, "Global Assimilation of Multiangle and Multipolarization SMOS Brightness Temperature Observations into the GEOS-5 Catchment Land Surface Model for Soil Moisture Estimation," *Journal of Hydrometeorology*, vol. 17, no. 2, pp. 669–691, Feb. 2016.

[51] R. H. Reichle, G. J. M. De Lannoy, Q. Liu, R. D. Koster, J. S. Kimball, W. T. Crow, J. V. Ardizzone, P. Chakraborty, D. W. Collins, A. L. Conaty, M. Girotto, L. A. Jones, J. Kolassa, H. Lievens, R. A. Lucchesi, and E. B. Smith, "Global Assessment of the SMAP Level-4 Surface and Root-Zone Soil Moisture Product Using Assimilation Diagnostics," *Journal of Hydrometeorology*, vol. 18, no. 12, pp. 3217–3237, Dec. 2017.

[52] R. D. Koster, M. J. Suarez, A. Ducharne, M. Stieglitz, and P. Kumar, "A catchment-based approach to modeling land surface processes in a general circulation model: 1. Model structure," *Journal of Geophysical Research: Atmospheres*, vol. 105, no. D20, pp. 24809–24822, Oct. 2000.

[53] A. Ducharne, R. D. Koster, M. J. Suarez, M. Stieglitz, and P. Kumar, "A catchment-based approach to modeling land surface processes in a general circulation model: 2. Parameter estimation and model demonstration," *Journal of Geophysical Research: Atmospheres*, vol. 105, no. D20, pp. 24823–24838, Oct. 2000.

[54] M. Stieglitz, A. Ducharne, R. Koster, and M. Suarez, "The Impact of Detailed Snow Physics on the Simulation of Snow Cover and Subsurface Thermodynamics at Continental Scales," *Journal of Hydrometeorology*, vol. 2, no. 3, pp. 228–242, Jun. 2001.

[55] G. J. M. De Lannoy, R. H. Reichle, and V. R. N. Pauwels, "Global Calibration of the GEOS-5 L-Band Microwave Radiative Transfer Model over Nonfrozen Land Using SMOS Observations," *Journal of Hydrometeorology*, vol. 14, no. 3, pp. 765–785, Jun. 2013.

[56] G. J. M. De Lannoy, R. H. Reichle, and J. A. Vrugt, "Uncertainty quantification of GEOS-5 L-band radiative transfer model parameters using Bayesian inference and SMOS observations," *Remote Sensing of Environment*, vol. 148, pp. 146–157, May 2014.

[57] D. Entekhabi, R. H. Reichle, R. D. Koster, and W. T. Crow, "Performance Metrics for Soil Moisture Retrievals and Application Requirements," *Journal of Hydrometeorology*, vol. 11, no. 3, pp. 832–840, Jun. 2010.

[58] F. Chen, W. T. Crow, M. H. Cosh, A. Colliander, J. Asanuma, A. Berg, D. D. Bosch, T. G. Caldwell, C. H. Collins, K. H. Jensen, J. Martínez-Fernández, H. McNairn, P. J. Starks, Z. Su, and J. P. Walker, "Uncertainty of Reference Pixel Soil Moisture Averages Sampled at SMAP Core Validation Sites," *Journal of Hydrometeorology*, vol. 20, no. 8, pp. 1553–1569, Jul. 2019.

[59] M. H. Cosh, T. J. Jackson, P. Starks, and G. Heathman, "Temporal stability of surface soil moisture in the Little Washita River watershed and its applications in satellite soil moisture product

validation," *Journal of Hydrology*, vol. 323, no. 1–4, pp. 168–177, May 2006.

[60] D. D. Bosch, J. M. Sheridan, and L. K. Marshall, "Precipitation, soil moisture, and climate database, Little River Experimental Watershed, Georgia, United States," *Water Resources Research*, vol. 43, no. 9, Sep. 2007.

[61] T. O. Keefer, M. S. Moran, and G. B. Paige, "Long-term meteorological and soil hydrology database, Walnut Gulch Experimental Watershed, Arizona, United States," *Water Resources Research*, vol. 44, no. 5, Mar. 2008.

[62] S. Bircher, N. Skou, K. H. Jensen, J. P. Walker, and L. Rasmussen, "A soil moisture and temperature network for SMOS validation in Western Denmark," *Hydrology and Earth System Sciences*, vol. 16, no. 5, pp. 1445–1463, May 2012.

[63] N. Sanchez, J. Martinez-Fernandez, A. Scaini, and C. Perez-Gutierrez, "Validation of the SMOS L2 Soil Moisture Data in the REMEDHUS Network (Spain)," *IEEE Transactions on Geoscience and Remote Sensing*, vol. 50, no. 5, pp. 1602–1611, May 2012.

[64] M. H. Cosh, P. J. Starks, J. A. Guzman, and D. N. Moriasi, "Upper Washita River Experimental Watersheds: Multiyear Stability of Soil Water Content Profiles," *Journal of Environmental Quality*, vol. 43, no. 4, pp. 1328–1333, Jul. 2014.

[65] R. Panciera, J. P. Walker, T. J. Jackson, D. A. Gray, M. A. Tanase, D. Ryu, A. Monerris, H. Yardley, C. Rudiger, X. Wu, Y. Gao, and J. M. Hacker, "The Soil Moisture Active Passive Experiments (SMAPEx): Toward Soil Moisture Retrieval From the SMAP Mission," *IEEE Transactions on Geoscience and Remote Sensing*, vol. 52, no. 1, pp. 490–507, Jan. 2014.

[66] E. J. Coopersmith, M. H. Cosh, W. A. Petersen, J. Prueger, and J. J. Niemeier, "Soil Moisture Model Calibration and Validation: An ARS Watershed on the South Fork Iowa River," *Journal of Hydrometeorology*, vol. 16, no. 3, pp. 1087–1101, May 2015.

[67] Á. González-Zamora, N. Sánchez, J. Martínez-Fernández, Á. Gumuzzio, M. Piles, and E. Olmedo, "Long-term SMOS soil moisture products: A comprehensive evaluation across scales and methods in the Duero Basin (Spain)," *Physics and Chemistry of the Earth*, Parts A/B/C, vol. 83–84, pp. 123–136, 2015.

[68] H. McNairn, T. J. Jackson, G. Wiseman, S. Belair, A. Berg, P. Bullock, A. Colliander, M. H. Cosh, S.-B. Kim, R. Magagi, M. Moghaddam, E. G. Njoku, J. R. Adams, S. Homayouni, E. Ojo, T. Rowlandson, J. Shang, K. Goita, and M. Hosseini, "The Soil Moisture Active Passive Validation Experiment 2012 (SMAPVEX12): Prelaunch Calibration and Validation of the SMAP Soil Moisture Algorithms," *IEEE Transactions on Geoscience and Remote Sensing*, vol. 53, no. 5, pp. 2784–2801, May 2015.

[69] T. Rowlandson, S. Impera, J. Belanger, A. A. Berg, B. Toth, and R. Magagi, "Use of in situ soil moisture network for estimating regional-scale soil moisture during high soil moisture conditions," *Canadian Water Resources Journal / Revue canadienne des ressources hydriques*, vol. 40, no. 4, pp. 343–351, Jul. 2015.

[70] A. Colliander, T. J. Jackson, R. Bindlish, S. Chan, N. Das, S. B. Kim, M. H. Cosh, R. S. Dunbar, L. Dang, L. Pashaian, J. Asanuma, K. Aida, A. Berg, T. Rowlandson, D. Bosch, T. Caldwell, K. Caylor, D. Goodrich, H. al Jassar, E. Lopez-Baeza, J. Martínez-Fernández, A. González-Zamora, S. Livingston, H. McNairn, A. Pacheco, M. Moghaddam, C. Montzka, C. Notarnicola, G. Niedrist, T. Pellarin, J. Prueger, J. Pulliainen, K. Rautiainen, J. Ramos, M. Seyfried, P. Starks, Z. Su, Y. Zeng, R. van der Velde, M. Thibeault, W. Dorigo, M. Vreugdenhil, J. P. Walker, X. Wu, A. Monerris, P. E. O'Neill, D. Entekhabi, E. G.

Njoku, and S. Yueh, "Validation of SMAP surface soil moisture products with core validation sites," *Remote Sensing of Environment*, vol. 191, pp. 215–231, Mar. 2017.

[71] A. Colliander, J. Asanuma, A. Berg, T. Bongiovanni, D. Bosch, T. Caldwell, M. Cosh, C. Holified-Collins, K. Jensen, S. Livingston, E. Lopez-Baeza, J. Martinez-Fernandez, H. McNairn, J. Prueger, M. Seyfried, P. Starks, Z. Su, M. Thibeault, and J. Walker, "SMAP/In Situ Core Validation Site Land Surface Parameters Match-Up Data, Version 1." *NASA National Snow and Ice Data Center DAAC*, 2017, doi: 10.5067/DXAVIXLY18KM.

[72] T. G. Caldwell, T. Bongiovanni, M. H. Cosh, C. Halley, and M. H. Young, "Field and Laboratory Evaluation of the CS655 Soil Water Content Sensor," *Vadose Zone Journal*, vol. 17, no. 1, p. 170214, 2018.

[73] K. H. Jensen and J. C. Refsgaard, "HOBE: The Danish Hydrological Observatory," *Vadose Zone Journal*, vol. 17, no. 1, p. 180059, 2018.

[74] E. Tetlock, B. Toth, A. Berg, T. Rowlandson, and J. T. Ambadan, "An 11-year (2007–2017) soil moisture and precipitation dataset from the Kenaston Network in the Brightwater Creek basin, Saskatchewan, Canada," *Earth System Science Data*, vol. 11, no. 2, pp. 787–796, Jun. 2019.

[75] G. L. Schaefer, M. H. Cosh, and T. J. Jackson, "The USDA Natural Resources Conservation Service Soil Climate Analysis Network (SCAN)," *Journal of Atmospheric and Oceanic Technology*, vol. 24, no. 12, pp. 2073–2077, Dec. 2007.

[76] J. E. Bell, M. A. Palecki, C. B. Baker, W. G. Collins, J. H. Lawrimore, R. D. Leeper, M. E. Hall, J. Kochendorfer, T. P. Meyers, T. Wilson, and H. J. Diamond, "U.S. Climate Reference Network Soil Moisture and Temperature Observations," *Journal of Hydrometeorology*, vol. 14, no. 3, pp. 977–988, Jun. 2013.

[77] H. J. Diamond, T. R. Karl, M. A. Palecki, C. B. Baker, J. E. Bell, R. D. Leeper, D. R. Easterling, J. H. Lawrimore, T. P. Meyers, M. R. Helfert, G. Goodge, and P. W. Thorne, "U.S. Climate Reference Network after One Decade of Operations: Status and Assessment," *Bulletin of the American Meteorological Society*, vol. 94, no. 4, pp. 485–498, Apr. 2013.

[78] R. A. McPherson, C. A. Fiebrich, K. C. Crawford, J. R. Kilby, D. L. Grimsley, J. E. Martinez, J. B. Basara, B. G. Illston, D. A. Morris, K. A. Kloesel, A. D. Melvin, H. Shrivastava, J. M. Wolfinbarger, J. P. Bostic, D. B. Demko, R. L. Elliott, S. J. Stadler, J. D. Carlson, and A. J. Sutherland, "Statewide Monitoring of the Mesoscale Environment: A Technical Update on the Oklahoma Mesonet," *Journal of Atmospheric and Oceanic Technology*, vol. 24, no. 3, pp. 301–321, Mar. 2007.

[79] J.-C. Calvet, N. Fritz, F. Froissard, D. Suquia, A. Petitpa, and B. Piguet, "In situ soil moisture observations for the CAL/VAL of SMOS: the SMOSMANIA network," *2007 IEEE International Geoscience and Remote Sensing Symposium*, 2007.

[80] A. B. Smith, J. P. Walker, A. W. Western, R. I. Young, K. M. Ellett, R. C. Pipunic, R. B. Grayson, L. Siriwardena, F. H. S. Chiew, and H. Richter, "The Murrumbidgee soil moisture monitoring network data set," *Water Resources Research*, vol. 48, no. 7, Jul. 2012.

[81] R. H. Reichle, Q. Liu, R. D. Koster, J. V. Ardizzone, A. Colliander, W. T. Crow, G. J. M. De Lannoy, and J. S. Kimball, "Soil Moisture Active Passive (SMAP) Project Assessment Report for Version 4 of the L4_SM Data Product", NASA Technical Report Series on Global Modeling and Data Assimilation, NASA/TM-2018-104606, Vol. 52, 72 pp, 2018. [Online]. Available: http://gmao.gsfc.nasa.gov/publications.

[82] A. Smith, N. Lott, and R. Vose, "The Integrated Surface Database: Recent Developments and Partnerships," *Bulletin of the American Meteorological Society*, vol. 92, no. 6, pp. 704–708, Jun. 2011.

[83] R. J. H. Dunn, K. M. Willett, D. E. Parker, and L. Mitchell, "Expanding HadISD: quality-controlled, sub-daily station data from 1931," *Geoscientific Instrumentation, Methods and Data Systems*, vol. 5, no. 2, pp. 473–491, Sep. 2016.

[84] M. J. Menne, C. N. Williams, B. E. Gleason, J. J. Rennie, and J. H. Lawrimore, "The Global Historical Climatology Network Monthly Temperature Dataset, Version 4," *Journal of Climate*, vol. 31, no. 24, pp. 9835–9854, Dec. 2018.

[85] H. van Velthuizen, B. Huddleston, G. Fischer, M. Salvatore, E. Ataman, F.O. Nachtergaele, M. Zanetti, and M. Bloise, "Annex II: Global land cover and availability of land for rainfed agriculture", in Mapping biophysical factors that influence agricultural production and rural vulnerability, Rome, Italy: *Food and Agriculture Organization of the United Nations and the International Institute of Applied Systems Analysis*, Environment and Natural Resources Series No. 11, 2007, pp. 49-56, ISBN 978-92-5-105689-9, ISSN 1684-8241. [Online]. Available: http://www.fao.org/3/a1075e/a1075e00.htm.

[86] P. A. Dirmeyer, L. Chen, J. Wu, C.-S. Shin, B. Huang, B. A. Cash, M. G. Bosilovich, S. Mahanama, R. D. Koster, J. A. Santanello, M. B. Ek, G. Balsamo, E. Dutra, and D. M. Lawrence, "Verification of Land–Atmosphere Coupling in Forecast Models, Reanalyses, and Land Surface Models Using Flux Site Observations," *Journal of Hydrometeorology*, vol. 19, no. 2, pp. 375–392, Feb. 2018.

[87] W. T. Crow, C. Arroyo Gomez, J. Muñoz Sabater, T. Holmes, C. R. Hain, F. Lei, J. Dong, J. G. Alfieri, and M. C. Anderson, "Soil Moisture–Evapotranspiration Overcoupling and L-Band Brightness Temperature Assimilation: Sources and Forecast Implications," *Journal of Hydrometeorology*, vol. 21, no. 10, pp. 2359–2374, Oct. 2020.

[88] R. Todling and A. El Akkraoui, "The GMAO Hybrid Ensemble-Variational Atmospheric Data Assimilation System: Version 2.0.", NASA Technical Report Series on Global Modeling and Data Assimilation, NASA/TM-2018-104606, Vol. 50, 184 pp, 2018. [Online]. Available: http://gmao.gsfc.nasa.gov/publications.

[89] C. S. Draper, "Accounting for land model error in numerical weather prediction ensemble systems: toward ensemble-based coupled land/atmosphere data assimilation," *Journal of Hydrometeorology*, Jun. 2021, vol. 22, no. 8, pp. 2089–2104.

Rolf H. Reichle received the M.S. degree ("Diplom") in physics from the University of Heidelberg, Heidelberg, Germany, in 1996, and the Ph.D. degree in environmental engineering from the Massachusetts Institute of Technology, Cambridge, MA, USA, in 2000. He is currently a Research Physical Scientist with the Global Modeling and Assimilation Office, NASA Goddard Space Flight Center, Greenbelt, MD, USA. His research interests include land data assimilation, satellite-based remote sensing, and applications related to land-atmosphere interactions, weather prediction, and seasonal climate forecasting.

Sara Q. Zhang, photograph and biography not available at the time of publication.

Qing Liu, photograph and biography not available at the time of publication.

Clara S. Draper leads the development of land data assimilation for global numerical weather prediction (NWP) at NOAA. Her research is focused on land data assimilation, and includes developing algorithms and data assimilation coupling strategies, assimilation of novel observations, and evaluating and understanding the role of land data assimilation in atmospheric prediction across a range of time scales. Her current projects include developing a coupled land/atmosphere data assimilation system for NOAA's Unified Forecast System (UFS) NWP system, modernizing the UFS snow data assimilation system, and improving the assimilation of SMAP soil moisture observations into numerical weather prediction models.

Jana Kolassa is a researcher and scientific land model developer at the Global Modeling and Assimilation Office (GMAO) at the NASA Goddard Space Flight Center. She obtained her PhD in Environmental Science and Remote Sensing from the Université Pierre et Marie Curie in 2013. Before joining the GMAO as a full-time researcher, she worked as a postdoctoral fellow at Columbia University in New York and through the NASA Postdoctoral Program. Her research focuses on improving the representation on land-atmosphere interaction in global Earth System Models through improvements in process representation and data assimilation. She is currently developing the next version of the NASA Catchment-CN model and is leading a project that investigates the potential of SMAP soil moisture data assimilation to improve the forecast of tropical cyclone landfall behavior in the GMAO's operational GEOS model.

Ricardo Todling started at the NASA Data Assimilation Office under a National Research Council fellowship in 1992, followed by a fellowship from the Universities Space Research Association in 1994, and subsequently joined Science Applications International Corporation as a contractor working for NASA's DAO and its successor, the Global Modeling and Assimilation Office (GMAO). In 2009, Dr. Todling was hired as a civil servant working for NASA/GMAO as Research Meteorologist.

Since 1996, Dr. Todling has been directly involved in developments associated with the DAO and GMAO data assimilation systems. He is one of the primary developers of the first NASA/DAO near-real-time data assimilation system built to support NASA's Earth Observing System program in the late 1990's and beyond. Since then, he has been leading data assimilation development in the Goddard Earth Observing System. This system provides data for NASA Instrument Teams to validate and calibrate their products and also supports the Modern-Era Retrospective analysis for Research and Applications. Dr. Todling has served as liaison between GMAO and NOAA's National Centers for Environmental Prediction since the initial days of GMAO. He has directly contributed to the development of the Gridpoint Statistical Interpolation analysis system; this is the system supporting data assimilation efforts at GMAO, NCEP and their Joint Center for Satellite Data Assimilation partners. More recently, Dr. Todling has led the development and implementation of the GMAO Hybrid four-dimensional Ensemble-Variational Data Assimilation System. Dr. Todling has also been the lead developer of the GMAO adjoint-based tool for assessing observation impact to forecasts. More recently, Dr. Todling has been involved in testing components of JEDI, the future NASA/NOAA data assimilation system.

TABLE I
EXPERIMENT OVERVIEW.

Experiment name	System or subsystem; model	Analysis algorithm[a]	Assimilated observations	Surface meteorological forcing	Experiment period	Start of spin-up period	Model initial conditions: Atmosphere	Land
ADAS	ADAS; AGCM	3D-Var	Operational FP data stream	ADAS AGCM (Corrector)	JJA 2017	1 Apr 2017	MERRA-2	Land model spin-up
LADAS	ADAS; AGCM	3D-Var	Operational FP data stream	LADAS AGCM (Corrector)	JJA 2017	3 May 2017	ADAS experiment	ADAS experiment
	LDAS; Catchment	EnKF (Nens=24)	SMAP Tb	LADAS AGCM (Predictor)	JJA 2017	3 May 2017	n/a	LDAS Open Loop
LDASoffl	LDAS; Catchment	EnKF (Nens=24)	SMAP Tb	ADAS (Predictor)	JJA 2017	n/a	n/a	LADAS experiment
LDAS Open Loop	LDAS; Catchment	n/a (Nens=24)	n/a	FP (Corrector)	Apr 2015– Apr 2020	1 Jan 2015 (ensemble)	n/a	Land model spin-up

ADAS and LADAS output examined in this study is from the AGCM Corrector segment.

[a]Number of land ensemble members is denoted with N_{ens}.
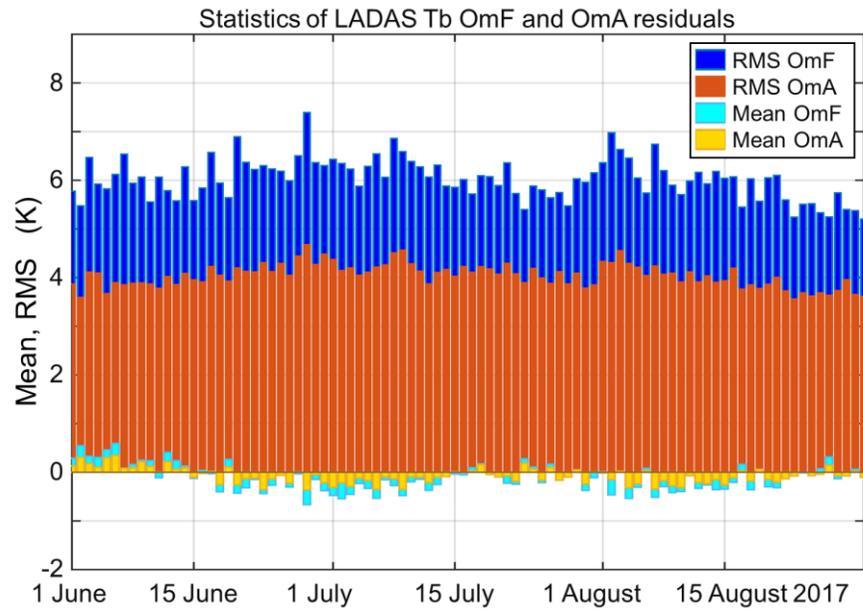
Fig. 1. Daily global mean and RMS of L-band Tb observation-minus-forecast (OmF) and observation-minus-analysis (OmA) residuals from the LDAS subsystem in the LADAS experiment for JJA 2017. OmF and OmA residuals computed after climatological rescaling of SMAP Tb observations.

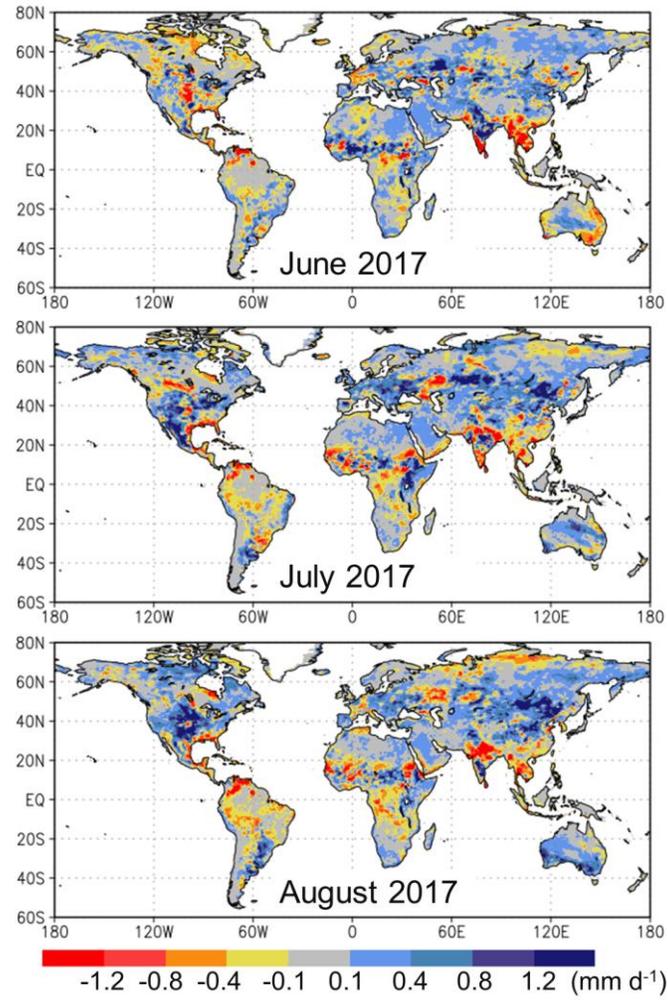## Monthly Mean Profile Soil Moisture Increments

Fig. 2. Monthly mean of ensemble-average profile soil moisture increments in equivalent flux units (mm d^{-1}) in the LADAS experiment for (a) June, (b) July, and (c) August 2017.
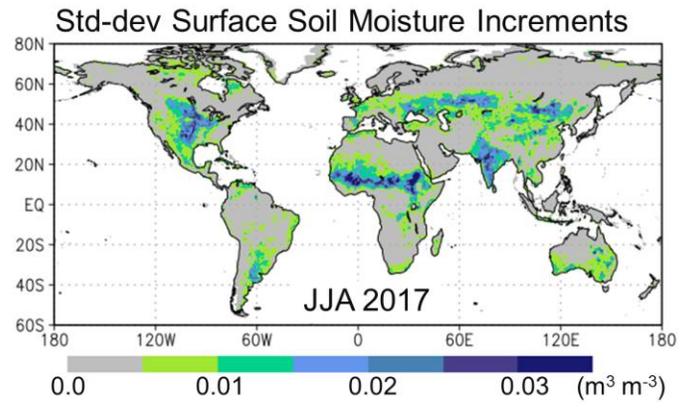
Fig. 3. Time series standard deviation of ensemble-average analysis increments for surface soil moisture ($m^3 m^{-3}$) in the LADAS experiment for JJA 2017.
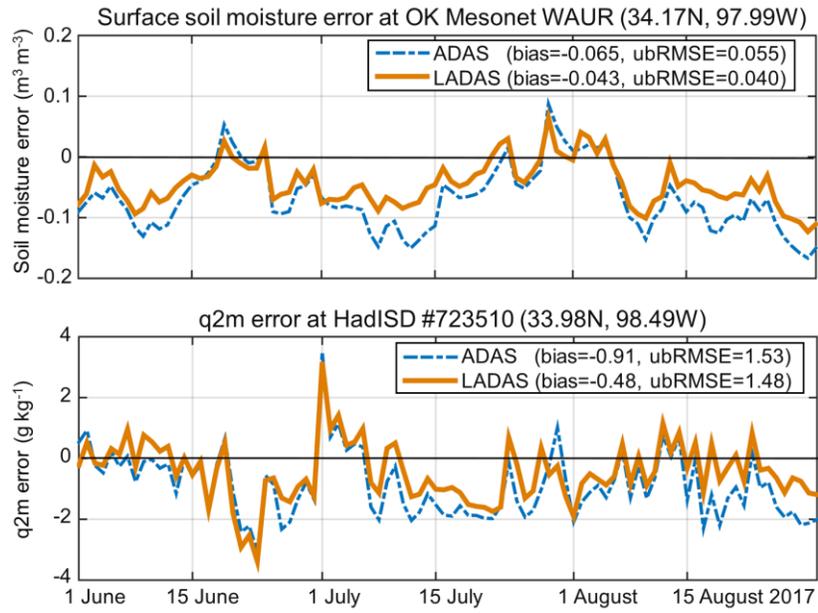
Fig. 4. Daily averaged analysis error (model minus measurement) for (a) surface soil moisture (m^3 m^{-3}) and (b) q2m (g kg^{-1}) from the (dashed blue lines) ADAS control and (solid brown lines) LADAS experiments near 34N, 98W in Oklahoma US for JJA 2017. Error computed vs. in situ measurements from the Oklahoma Mesonet Waurika station for soil moisture and from HadISD station #723510 for q2m.
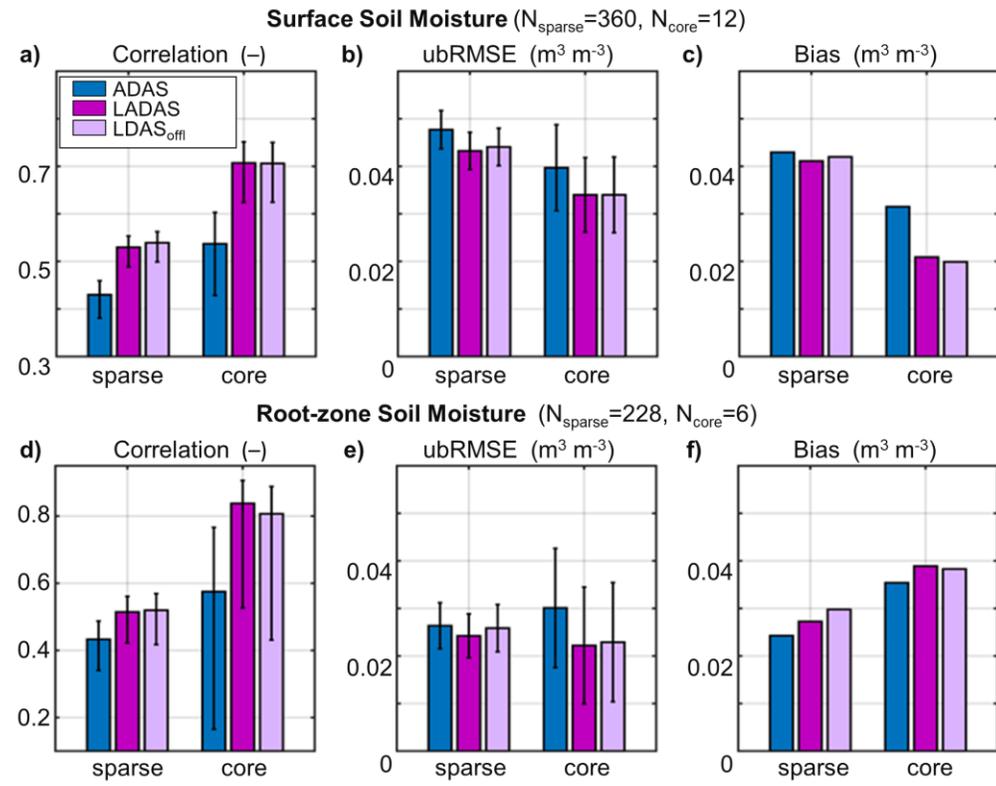
Fig. 5. (a,d) Correlation (dimensionless), (b,e) ubRMSE (m³ m⁻³), and (c,f) bias (model minus measurement; m³ m⁻³) for (a-c) surface and (d-f) root-zone soil moisture from the ADAS control, LADAS, and LDAS$_{offl}$ experiments. Metrics are computed vs. in situ measurements from sparse networks (first group of bars) and SMAP core validation sites (second group of bars) for JJA 2017. N_{sparse} and N_{core} indicate the number of sites used to compute the metrics. Error bars indicate 95% confidence intervals (see text for details). Note that the sparse network and core sites differ in their coverage across land surface conditions and climate zones.
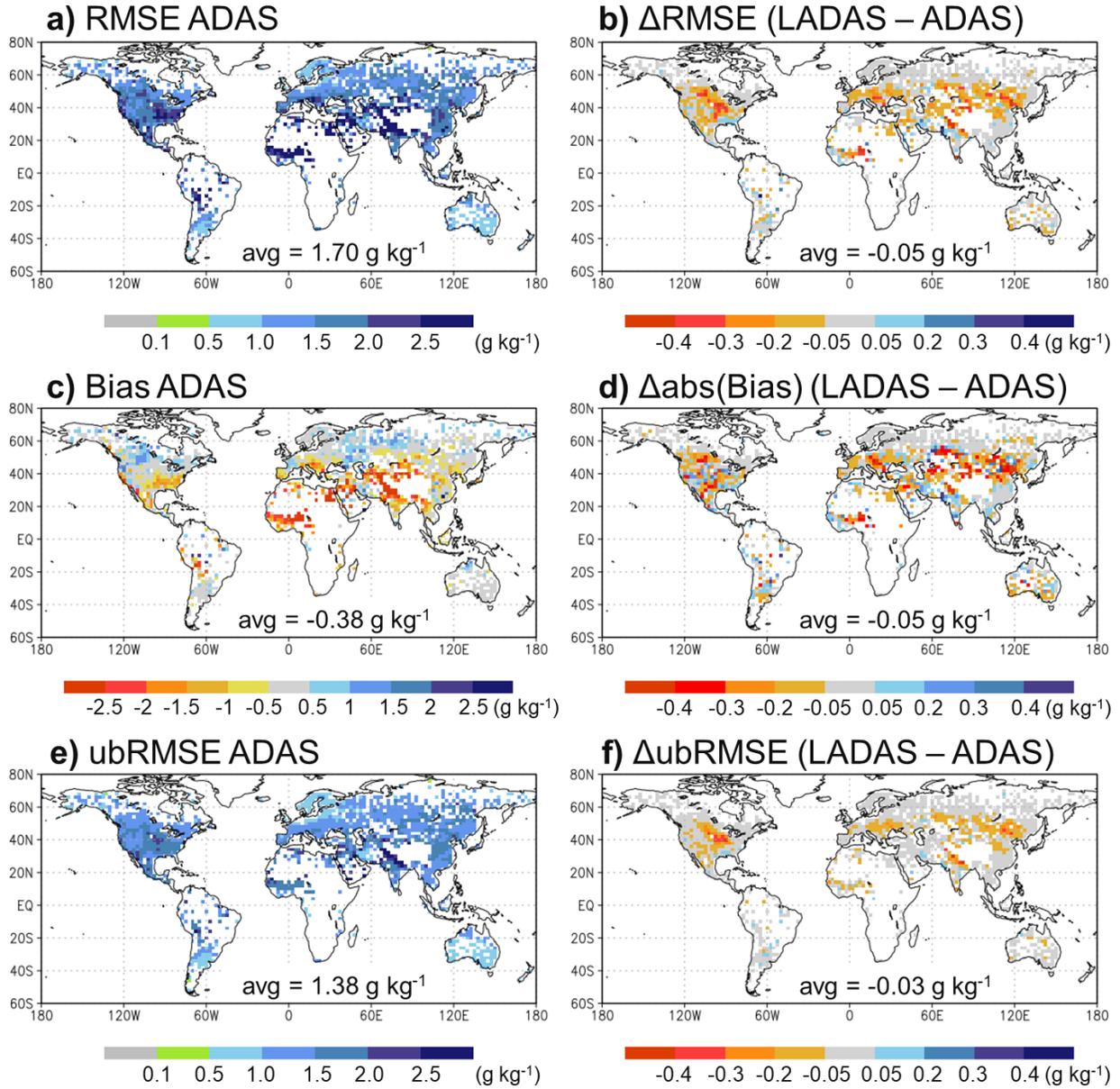
q2m metrics vs. HadISD

Fig. 6. Left column shows (a) RMSE, (c) bias (model minus measurement), and (e) ubRMSE of 2-m specific humidity from the ADAS control experiment vs. HadISD measurements. Right column shows LADAS-minus-ADAS difference in the performance statistics for (b) RMSE, (d) absolute bias, and (f) ubRMSE, with red colors in (b,d,f) indicating that LADAS has better skill than ADAS. All statistics are calculated for JJA 2017.

T2m$_{max}$ metrics vs. GHCN

a) RMSE ADAS

avg = 2.77 K

b) ΔRMSE (LADAS – ADAS)

avg = -0.04 K

c) Bias ADAS

avg = -0.70 K

d) Δabs(Bias) (LADAS – ADAS)

avg = -0.02 K

e) ubRMSE ADAS

avg = 1.77 K

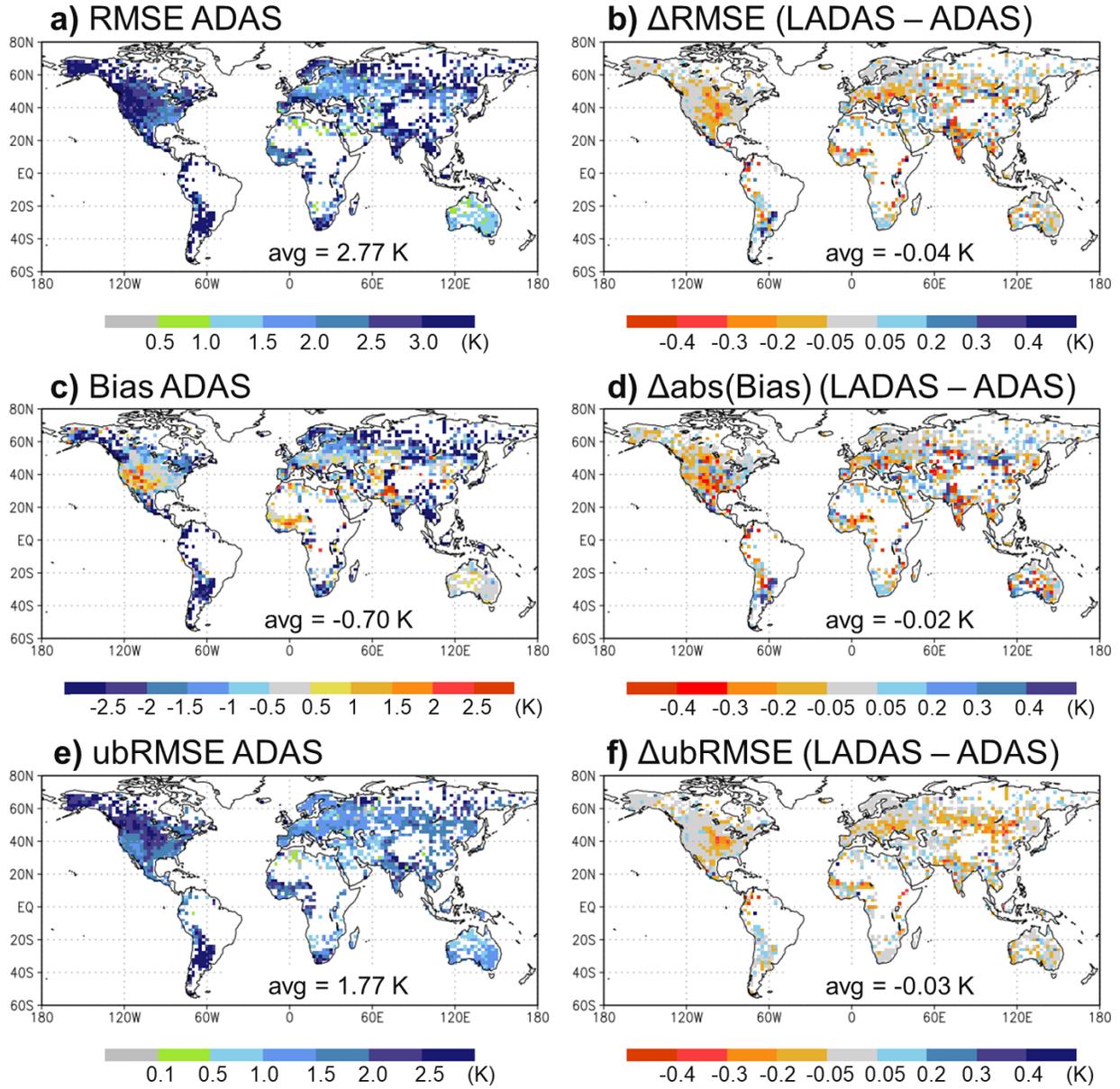**f)** ΔubRMSE (LADAS – ADAS)

avg = -0.03 K

Fig. 7. As in Fig. 6 but for 2-m maximum daily air temperature evaluated against GHCN measurements.
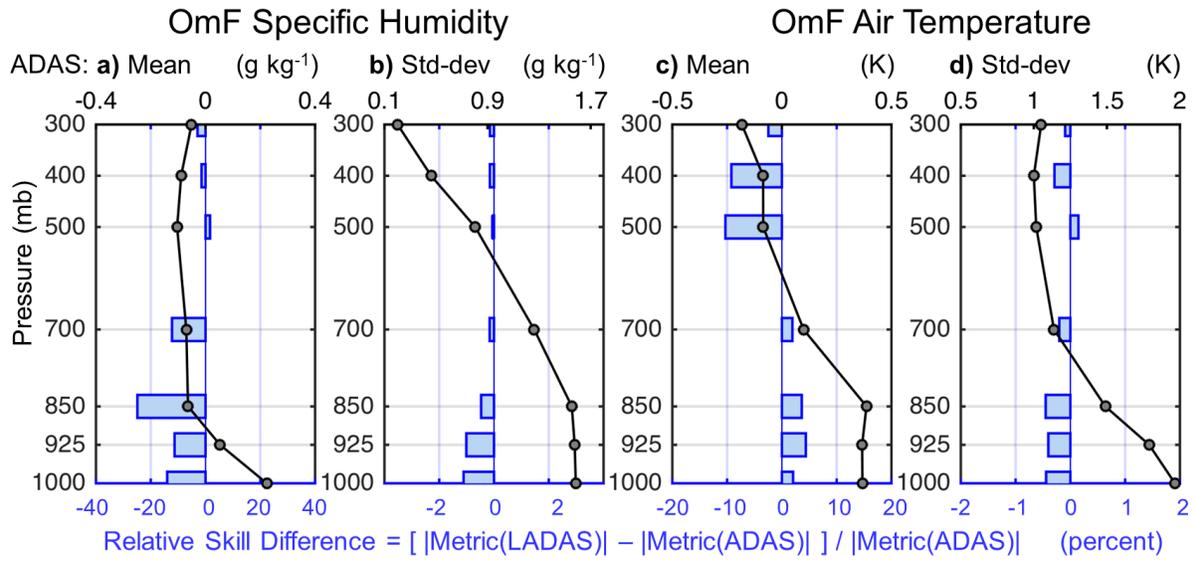
Fig. 8. Black dots show atmospheric profiles of the (a,c) mean and (b,d) standard-deviation of OmF residuals from the ADAS control experiment for (a,b) specific humidity (g kg^{-1}) and (c,d) air temperature (K) across global continental land for JJA 2017. OmF residuals were computed using radiosonde observations. Blue bars indicate corresponding relative skill difference (LADAS vs. ADAS) in OmF (a,c) absolute mean and (b,d) standard deviation in units of percent. Blue bars with negative (positive) percentage values indicate better (worse) performance of LADAS compared to ADAS.
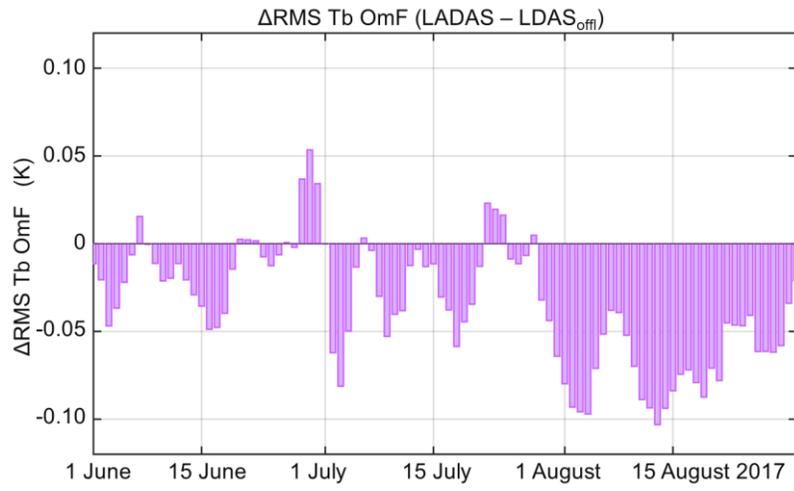
Fig. 9. Daily RMS of SMAP Tb observation-minus-forecast residuals from LADAS minus same from LDAS$_{offl}$ for JJA 2017. Negative values indicate that the Tb background forecasts in the LADAS are closer to the SMAP Tb observations than are those of the LDAS$_{offl}$ experiment.